Received: 12 April 2023 | Revised: 4 September 2023 | Accepted: 15 November 2023

DOI: 10.1002/mma.9823

RESEARCH ARTICLE

WILEY

Mathematical fundamentals of spherical kinematics of plate tectonics in terms of quaternions

Helmut Schaeben[1] | **Uwe Kroner**[2] | **Tobias Stephan**[3,4]

[1]Department of Geophysics and Geoinformatics, TU Bergakademie Freiberg, Freiberg, Germany

[2]Department of Geology, TU Bergakademie Freiberg, Freiberg, Germany

[3]Department of Geoscience, University of Calgary, Calgary, Alberta, Canada

[4]Department of Geology, Lakehead University, Thunder Bay Campus, Thunder Bay, Ontario, Canada

Correspondence
Helmut Schaeben, Department of Geophysics and Geoinformatics, TU Bergakademie Freiberg, Germany.
Email: schaeben@tu-freiberg.de

Communicated by: W. Sproessig

To be a quantitative and testable tectonic model, plate tectonics requires spherical geometry and spherical kinematics in terms of finite rotations conveniently parametrized by their angle and axis and described by unit quaternions. In treatises on "Plate Tectonics" infinitesimal, instantaneous, and finite rotations, absolute and relative rotations are said to be applied to model the motion of tectonic plates. Even though these terms are strictly defined in mathematics, they are often casually used in geosciences. Here, their definitions are recalled and clarified as well as the terms rotation, orientation, and location on the sphere. For instance, infinitesimal rotations refer to a mathematical limit, when the angle of rotation tends to zero. Their rules do not apply to finite rotations, no matter how small their finite angles of rotation are. Mathematical approaches applying appropriate and feasible assumptions to model spherical motion of tectonic plates over geological times of hundreds of millions of years are derived including (i) sequences of incremental finite rotations, (ii) sequences of accumulating successive concatenations of finite rotations, and (iii) continuous rotations in terms of fully transient quaternions. The incremental and the accumulating approaches provide complementary views. While the relative Euler pole appears to migrate in the latter, it appears fixed in the former. Path, mean, and instantaneous velocity of the migrating Euler pole are derived as well as the angular and trajectoral velocity of the rotational motion about it. The approaches are illustrated by a geological example with actual data and a numerical yet geologically inspired example with artificial data. The former revisits the three-plate scenario with stationary axes of two "absolute" rotations implying transient "relative" rotations about a migrating Euler pole and employs a proper plate-circuit argument to determine them numerically without resorting to approximations. The latter applies an involved interplay of incremental and accumulating modeling inducing split–join cycles to approximate sinusoidal trajectories as reported to record plates' motion during the Gondwana breakup.

KEYWORDS

absolute versus relative rotation, concatenation of rotations, continuous rotation, continuous rotational motion on the sphere, Euler pole, finite rotation, migrating Euler pole, piecewise rotational motion on the sphere, plate tectonics, quaternion, Rodrigues' formula, Rodrigues vector, sinusoidal trajectories, spatial reference, successive incremental rotations, successively accumulated total rotations, tectonic plate circuit, transient quaternion

MSC CLASSIFICATION

70B10, 86A60

1 | INTRODUCTION

In his afterthoughts of a witness, Le Pichon [1] remembers

> The essence of Plate Tectonics, in my opinion, is that it is the first quantitative tectonic model. And it is impossible to quantify the motion of plates on the Earth using plane geometry. ([1, p. 14])
>
> …
>
> It was recognizing that, without it [spherical geometry, these authors], instantaneous and finite kinematics on the Earth were doomed. ([1, p. 14])
>
> …
>
> Although, moving from plane to spherical geometry is a very simple step that required no new theory, it enabled Plate Tectonics to become quantitative and consequently testable. ([1, p. 15])

Up to the present, the groundbreaking treatise "Plate Tectonics" by Le Pichon et al. [2] is a major reference in the field and provides the introduction here. In their Chapter 4 "Kinematics of relative movements," the authors take a turn from "Instantaneous movements" (referring to infinitesimal rotation) to "Kinematics of finite motions" and state:

> lt is clear from geology that the plates carrying continents and oceans have moved more than by an infinitely small amount. Most of the theory developed to treat the problem of present-day tectonics in terms of instantaneous motions is therefore of no use in attempting to reconstruct the past positions of continents and oceans.
>
> When confronted with the problem of describing the displacements of plates for long periods of time two aspects have to be raised. First, it is necessary to use an accurate method to apply large displacements to the plates on a spherical earth and to know how to apply successive rotations to the plates and how to compose these rotations. (cf. Le Pichon et al. [2, p. 33])

Here, we present the required accurate method on a spherical (as opposed to a plane) Earth including successive concatenation of finite rotations in terms of quaternions.

Le Pichon et al. continue:

> In practice all workers in the field had to assume that for some finite time interval, the motion between two plates could be described by a single pole of rotation: …
>
> It is clear from these remarks that the assumption of constant relative motion commonly made in papers devoted to plate tectonics is a convenient way to escape the geometrical difficulties posed by the evolution of plates to which finite displacements are applied. (cf. Le Pichon et al. [2, p. 34]).

While this assumption seems actually inevitable if finite motions are modeled applying successive concatenation of finite rotations, it becomes obsolete when we proceed here to continuous rotations—in terms of quaternions, of course.

> As we have stated above, a rigorous method of treating finite rotations is needed to apply large displacements to the plates. (cf. Le Pichon et al. [2, p. 34]).

Their presentation of a "Theory of finite rotations" [2, pp. 34–37] graphically refers to Rodrigues' geometrical construction to compose finite rotations on the sphere [3] and uses (3×3) matrices of SO(3), to conclude eventually that the quaternion representation of rotations provides a most concise development, compare [2, p. 37], without elaborating on it.

Having the mathematical fundamentals right is the foremost prerequisite for proper, that is, mathematically approvable, models of the kinematics of plate tectonics and beyond. Here, we set out to present mathematical fundamentals to model the kinematics of motion of tectonic plates on the sphere featuring both sequences of finite rotations and continuous rotation in terms of quaternions. Following Le Pichon's approach of search for poles of rotation, computing vectors of motion along a plate boundary from the vector of rotation, and combination of instantaneous and finite rotations [1, p. 16] enabled for example a numerical model of early Paleozoic plate tectonics including a quantification of the relative rotation of Gondwana with respect to North America, and the approximation of patterns of sinusoidal trajectories of plate motion as observed with respect to the Gondwana breakup.

2 | ROTATIONS, ORIENTATIONS, AND EULER POLES

A finite rotation $R(\omega, \mathbf{e})$, conveniently parametrized here in terms of a finite angle $\omega \in (-\pi, \pi]$ and an axis of rotation $\{+\mathbf{e}, -\mathbf{e}\}$ provided by a unit vector $\mathbf{e} \in \mathbb{S}^2 \subset \mathbb{R}^3$ such that $R(\omega, \mathbf{e}) = R(-\omega, -\mathbf{e})$, is a mathematical operation, an instantaneous transformation, the application of which to an object changes its rotational state, that is, its orientation with respect to a given reference frame. Largely following the notation and conventions of [4, pp. 4–6], the symbol $\mathbf{e}$ casually denotes both the unit vector and the associated axis. A rotation is defined to be positive (negative) if it is seen counterclockwise (clockwise) from outside the unit sphere. The rotational axis passes through the center of the unit sphere modeling the Earth's shape and intersects the sphere at two antipodal points denoted by $\pm\mathbf{e} \in \mathbb{S}^2$, too, which remain invariant by the rotation $R(\omega, \mathbf{e})$. The point $\mathbf{e} \in \mathbb{S}^2$ is referred to as (Euler) pole of the rotation, if the rotation is seen counterclockwise from it; otherwise, the point $-\mathbf{e} \in \mathbb{S}^2$ is referred to as (Euler) pole of the rotation. Since usually the upper hemisphere of the reference sphere is projected onto the unit disk and plotted for purposes of illustration, whichever point appears on the upper hemisphere is casually referred to as Euler pole in geological applications. The meaning of the common symbol $\mathbf{e}$—vector, axis, Euler pole—should always be clear from the context.

The rotation of a unit vector, $\mathbf{v} \in \mathbb{S}^2$, results in a unit vector, $R(\omega, \mathbf{e})\mathbf{v} = \mathbf{w} \in \mathbb{S}^2$, and the spherical distance $d_S(\mathbf{v}, \mathbf{w}) = \arccos(\mathbf{v} \cdot \mathbf{w}) \leq \omega$. Equality holds if and only if $\mathbf{v}$ is an element of the great circle with pole $\mathbf{e}$.

Since a rotation is an isometry, the orientation of a spherical polygon, for instance, also appears as its location on the sphere with respect to a given reference frame.

It should be noted that rotations and orientations can be quantified by the same set of parameters and are described by the same expression, for example, real unit quaternions $q \in \mathbb{S}^3 \subset \mathbb{H}$, the skew field of Hamiltonian quaternions [5], or (3×3) matrices of SO(3), the special orthogonal group of $\mathbb{R}^3$.

2.1 | Small angle approximations

Since rotational rates of tectonic plates, that is, angles of rotation in radians per 1 Ma, are small, small angle approximations of basic trigonometric functions such as

$$\sin\omega \approx \omega, \cos\omega \approx 1 - \frac{\omega^2}{2} \approx 1, \tan\omega \approx \omega \tag{1}$$

are applied whenever convenient. As a rule of thumb, these approximations are considered acceptable if the relative error is less than 1%, that is, for angles roughly less than 10° equal to 0.17 rad. For example, a most prominent application is that for sufficiently small rotation angles the rotation vector of the concatenation of two rotations is approximately equal to the sum of the rotation vectors of the rotations being concatenated. It originates from Rodrigues formula of concatenating rotations [3].

3 | MOTION ON THE SPHERE IN TERMS OF ROTATIONS

There are several options to proceed from rotation as (instantaneous) transformation of orientation of an object to motion in the plane or on the sphere provided by rotation. An initial non-technical exposition is given as follows here. Its detailed elaboration will be presented later using quaternions because they are most appropriate for the purpose, compare [6].

3.1 | Sequence of finite rotations

Exploiting the intuition of a rotational motion through time, the trajectories of the vertices of an object, for example, a spherical polygon, subject to a rotation $R(\omega, \mathbf{e})$ are arcs of circles along which the orientation of the polygon gradually changes until the final orientation $R(\omega, \mathbf{e})$ is reached. Then, a sequence of rotations can be seen to provide two slightly different simple models of piecewise circular motion on the sphere,

- either a sequence $R_1, R_2, \ldots, R_\ell, \ldots$ of incremental finite rotations $R_\ell, \ell \in \mathbb{N}$,
- or a sequence $R_1, (R_2 R_1), \ldots, (R_\ell \ldots R_2 R_1), \ldots$ of accumulated total rotations by successive concatenations of sequential finite rotations.

A sequence of incremental finite rotations applied to the corresponding consecutive orientations of a polygon provides a model of a piecewise circular motion of the polygon. The trajectories of its vertices are joint arcs of circles. If the axes of the consecutive incremental rotations are the same, then their incremental angles sum up, and the piecewise arcs of circles join to arcs of unique circles.

Successive concatenations of the finite rotations of a sequence applied to the initial orientation of a polygon at each step of the successive concatenation result in a sequence of accumulated total rotations providing another model of circular motion on the sphere. The trajectories of the vertices are arcs of different circles of increasing angular length for each of the successive concatenations. If the axes are the same for all rotations being concatenated, then the angles of the concatenated rotations sum up, and trajectories are arcs of unique circles.

To extend these geometric models to include rotational rate, that is, velocity, the rotations are assigned to a strictly increasing sequence of discrete temporal marks $\tau_0 < \tau_1 < \ldots < \tau_\ell < \ldots$, resulting in a temporally indexed sequence of rotations closer to the conception of a rotational motion. Given a fixed axis for all rotations, a constant angle of all rotations and equidistant temporal marks apply to model a rotational motion of constant rate. Otherwise, angles and axes of the rotations are piecewise constant functions of time with discontinuities at the temporal marks $\tau_\ell, \ell = 1, 2, \ldots$.

3.2 | Continuous rotation

The models in terms of sequences of finite rotations may be generalized by defining angle and axis of rotation as continuous functions of time resulting in a transient rotation $R(\omega(t), \mathbf{e}(t)),\ t \in [0, \infty)$; $R(\omega(t_0), \mathbf{e}(t_0))$ referring to a given instant t_0 denotes an instantaneous rotation or rather instantaneous orientation, given by its instantaneous angle $\omega(t_0)$ and axis $\mathbf{e}(t_0)$. Then, differential calculus applies and canonically results in a mathematical representation of rotational motion, including rotational and trajectoral velocity, that is, velocity along the circular path of motion.

3.3 | Infinitesimal rotation

Even though the notion of infinitesimal entities, for example, arbitrarily small numbers larger than 0, is apparently appealing to intuition, it has largely been abandoned in mathematical analysis in favor of the notion of limits, because what appears appealing leads to a fundamental mathematical problem, compare [7, 8]. Thus, an infinitesimal rotation $R(\delta\omega, \mathbf{e})$ has to be thought of in terms of the mathematical limit for $\delta\omega \to 0$, compare [4, p. 80]. The first-order approximation $\widetilde{R}(\delta\omega, \mathbf{e})\mathbf{u}$ of the corresponding transformation $R(\delta\omega, \mathbf{e})\mathbf{u}$ of $\mathbf{u} \in \mathbb{S}^2$ applies to describe the infinitesimal change of the orientation of an object, here $\mathbf{u} \in \mathbb{S}^2$. In this way, the notion of infinitesimal rotations gave rise to proceed from a rotation to an infinitesimal circular motion, in particular to the vector of angular velocity along the unit vector $\mathbf{e}$ and to the vector of trajectoral velocity orthogonal to $\mathbf{e}$ and tangential at $\mathbf{u}$ to the circular path corresponding to the rotation.

Infinitesimal rotations do not apply to change the orientation of a tectonic plate by a given finite angle of rotation whatever its fixed (small) size. However, the approximations of Equation (1) apply and prove most useful.

4 | ROTATIONS IN TERMS OF QUATERNIONS

The classical reference of this topic is [4], and an easy introduction is [9]. A real unit quaternion $q = (q_0 + \mathbf{q}) \in \mathbb{S}^3 \subset \mathbb{H}$ of the $3d$ unit sphere in the $4d$ skew field $\mathbb{H}$ with scalar part $q_0 \in \mathbb{R}$ and vector part $\mathbf{q} \in \mathbb{R}^3$ may be represented as

$$q = \cos\frac{\omega}{2} + \mathbf{e}\sin\frac{\omega}{2},$$

with an angle $\omega \in (-\pi, \pi]$ and a unit vector $\mathbf{e} \in \mathbb{S}^2 \subset \mathbb{R}^3$. Since $q \in \mathbb{S}^3$, its inverse is equal to its conjugate, $q^{-1} = q^* = q_0 - \mathbf{q}$. The angle ω and the unit vector $\mathbf{e}$ may be associated with a rotation $R(\omega, \mathbf{e})$ by the angle ω about the unit vector $\mathbf{e}$, where the vector $\omega\mathbf{e} = \boldsymbol{\omega}$ is referred to as rotation vector. To rotate a unit vector $\mathbf{u} \in \mathbb{S}^2$ by $R(\omega, \mathbf{e})$ to the unit vector $\mathbf{w} = R(\omega, \mathbf{e})\mathbf{u}$ quaternion multiplication; see Equation (3), from left with q and from right with its conjugate q^* applies

$$q \circ \mathbf{u} \circ q^* = \mathbf{w}, \tag{2}$$

where $\mathbf{u}, \mathbf{w}$ are read as pure quaternions, that is, quaternions with vanishing scalar parts. Equation (2) implies that the quaternions q and $-q$ correspond to the same rotation.

4.1 | Rodrigues' rotation formula

Quaternion multiplication of Equation (2) yields Rodrigues' formula for rotations in $\mathbb{R}^3$

$$\begin{aligned} R(\omega, \mathbf{e})\mathbf{u} &= \mathbf{u}\cos\omega + (\mathbf{e} \times \mathbf{u})\sin\omega + \mathbf{e}(\mathbf{e} \cdot \mathbf{u})(1 - \cos\omega) \\ &= \mathbf{u} + (\mathbf{e} \times \mathbf{u})\sin\omega + \mathbf{e} \times (\mathbf{e} \times \mathbf{u})\, 2\sin^2\frac{\omega}{2} \end{aligned}$$

[3] when written explicitly.

4.2 | Concatenation of rotations

Concatenation of the two rotations $R_1 = R(\omega_1, \mathbf{e}_1)$ followed by $R_2 = R(\omega_2, \mathbf{e}_2)$ yields the resulting rotation $R_2R_1 = R = R(\omega, \mathbf{e})$ given in terms of quaternions q_1 and q_2, respectively, by

$$q = q_2 \circ q_1 = q_{20}q_{10} - \mathbf{q}_2 \cdot \mathbf{q}_1 + q_{10}\mathbf{q}_2 + q_{20}\mathbf{q}_1 + \mathbf{q}_2 \times \mathbf{q}_1, \tag{3}$$

where $\mathbf{p} \cdot \mathbf{q}$ and $\mathbf{p} \times \mathbf{q}$ represent the standard inner and cross product in $\mathbb{R}^3$, with scalar and vector parts

$$\begin{aligned} \mathrm{Sc}(q_2q_1) &= q_{20}q_{10} - \mathbf{q}_2 \cdot \mathbf{q}_1, \\ \mathrm{Vec}(q_2q_1) &= q_{10}\mathbf{q}_2 + q_{20}\mathbf{q}_1 + \mathbf{q}_2 \times \mathbf{q}_1. \end{aligned}$$

Thus, angle and axis of the resulting rotation R are provided by

$$\begin{aligned} \omega(R_2R_1) &= 2\arccos\left(q_{20}q_{10} - \mathbf{q}_2 \cdot \mathbf{q}_1\right), \\ \mathbf{e}(R_2R_1) &= \frac{1}{\sin\frac{\omega}{2}}\left(q_{10}\mathbf{q}_2 + q_{20}\mathbf{q}_1 + \mathbf{q}_2 \times \mathbf{q}_1\right), \end{aligned}$$

or more explicitly in terms of the involved angles and axes

$$\omega(R_2R_1) = 2\arccos\left(\cos\frac{\omega_2}{2}\cos\frac{\omega_1}{2} - \sin\frac{\omega_2}{2}\sin\frac{\omega_1}{2}\,\mathbf{e}_2 \cdot \mathbf{e}_1\right), \tag{4}$$

$$\mathbf{e}(R_2R_1) = \frac{1}{\sin\frac{\omega}{2}}\left(\cos\frac{\omega_1}{2}\sin\frac{\omega_2}{2}\,\mathbf{e}_2 + \cos\frac{\omega_2}{2}\sin\frac{\omega_1}{2}\,\mathbf{e}_1 + \sin\frac{\omega_2}{2}\sin\frac{\omega_1}{2}\,(\mathbf{e}_2 \times \mathbf{e}_1)\right). \tag{5}$$

Since the cross product of the axes of rotations is involved in Equation (5) it is obvious that finite rotations do not generally commute, they commute only if they have a common axis of rotation; then, the angles of rotation just sum up.

If $\omega_2 = \pm\omega_1 = \pm\zeta$, then

$$\mathbf{e}(R_2R_1) = \frac{1}{\sin\frac{\omega}{2}}\left(\sin\frac{\zeta}{2}\cos\frac{\zeta}{2}\,(\mathbf{e}_1 \pm \mathbf{e}_2) + \sin^2\frac{\zeta}{2}\,(\pm(\mathbf{e}_2 \times \mathbf{e}_1))\right). \tag{6}$$

Closely related to the unit quaternion $q = \cos\frac{\omega}{2} + \sin\frac{\omega}{2}\mathbf{e}$ associated with the rotation $R(\omega, \mathbf{e})$ is its Rodrigues vector $\mathbf{r}$ defined as

$$\mathbf{r} = \tan\frac{\omega}{2}\mathbf{e}.$$

Rephrasing Equations (3)–(5) as

$$\begin{aligned}\cos\frac{\omega(R_2R_1)}{2} + \sin\frac{\omega(R_2R_1)}{2}\mathbf{e} = &\left(\cos\frac{\omega_2}{2}\cos\frac{\omega_1}{2} - \sin\frac{\omega_2}{2}\sin\frac{\omega_1}{2}\,\mathbf{e}_2\cdot\mathbf{e}_1\right)\\ &+\left(\cos\frac{\omega_1}{2}\sin\frac{\omega_2}{2}\,\mathbf{e}_2 + \cos\frac{\omega_2}{2}\sin\frac{\omega_1}{2}\,\mathbf{e}_1 + \sin\frac{\omega_2}{2}\sin\frac{\omega_1}{2}\,(\mathbf{e}_2\times\mathbf{e}_1)\right)\end{aligned}$$

and applying the spherical law of cosines

$$\cos\frac{\omega(R_2R_1)}{2} = \cos\frac{\omega_2}{2}\cos\frac{\omega_1}{2} - \sin\frac{\omega_2}{2}\sin\frac{\omega_1}{2}\,\mathbf{e}_2\cdot\mathbf{e}_1,$$

compare [10, eq. (8.87)] referring to spherical kinematics in terms of quaternions or [11, p. 247] in terms of plain spherical trigonometry, lead to

$$\begin{aligned}\tan\frac{\omega(R_2R_1)}{2}\,\mathbf{e}(R_2R_1) &= \frac{\tan\frac{\omega_2}{2}\,\mathbf{e}_2 + \tan\frac{\omega_1}{2}\,\mathbf{e}_1 + \tan\frac{\omega_2}{2}\tan\frac{\omega_1}{2}\,(\mathbf{e}_2\times\mathbf{e}_1)}{1 - \tan\frac{\omega_2}{2}\tan\frac{\omega_1}{2}\,\mathbf{e}_2\cdot\mathbf{e}_1}\\ &= \frac{\mathbf{r}_2 + \mathbf{r}_1 + \mathbf{r}_2\times\mathbf{r}_1}{1 - \mathbf{r}_2\cdot\mathbf{r}_1},\end{aligned}$$

expressing concatenation in terms of Rodrigues vectors [3]. The three axes $\mathbf{e}_1, \mathbf{e}_2, \mathbf{e}(R_2R_1)$ of the rotations $R_1, R_2, (R_2R_1)$ define a spherical triangle, whose interior angles are determined by the angles of these rotations.

For sufficiently small rotation angles, compare Equation (1), the approximation

$$\omega(R_2R_1)\,\mathbf{e}(R_2R_1) \approx \omega_1\,\mathbf{e}_1 + \omega_2\,\mathbf{e}_2, \tag{7}$$

in terms of rotation vectors holds. It implies that the normalized sum of the rotation vectors

$$\widehat{\mathbf{e}}(R_2R_1) = \frac{\omega_1\mathbf{e}_1 + \omega_2\mathbf{e}_2}{\|\omega_1\mathbf{e}_1 + \omega_2\mathbf{e}_2\|} \approx \mathbf{e}(R_2R_1) \tag{8}$$

approximates the rotation axis of the concatenation for sufficiently small angles of rotation.

4.3 | Spatial references: Absolute and relative rotations

4.3.1 | Geometry versus topology

Applying a unique rotation R to two different spherical polygons $P_1, P_2 \in \mathbb{S}^2$ transforms their orientations and changes their locations on the sphere with respect to a given reference frame, but it preserves their relative location, that is, their topological relationship. Given two different rotations R_ℓ, $\ell = 1, 2$, and applying them to the polygons P_ℓ, $\ell = 1, 2$, transforms their orientations according to $R_\ell P_\ell = P'_\ell$, $\ell = 1, 2$, and changes both their locations with respect to a given reference frame and their relative location. The rotations $R_1R_2^{-1}$ and its inverse $\left(R_1R_2^{-1}\right)^{-1} = R_2R_1^{-1}$ restore the initial topological relationship of P_1 and P_2

- in terms of R_1P_ℓ, $\ell = 1, 2$, according to

$$R_1R_2^{-1}P'_2 = R_1R_2^{-1}R_2P_2 = R_1P_2, \tag{9}$$

  with respect to R_1P_1, and
- in terms of R_2P_ℓ, $\ell = 1, 2$, according to

$$R_2R_1^{-1}P'_1 = R_2R_1^{-1}R_1P_1 = R_2P_1, \tag{10}$$

  with respect to R_2P_2.

4.3.2 | Reference frame—point of view: Relative rotation

Equation (9) implies

$$P_2' = R_2 P_2 = \left(R_2 R_1^{-1}\right) R_1 P_2, \tag{11}$$

featuring the point of view of watching P_2 being rotated to P_2' as provided from $P_1' = R_1 P_1$ considered to have been immobile. Analogously, Equation (10) implies

$$P_1' = R_1 P_1 = \left(R_1 R_2^{-1}\right) R_2 P_1, \tag{12}$$

featuring the point of view of watching P_1 being rotated to P_1' as provided from $P_2' = R_2 P_2$ considered to have been immobile, cf. Figure 1. The rotation $R_1 R_2^{-1}$ is casually referred to as relative rotation $R_{1|2}$ of the polygon P_1 with respect to the point of view from polygon P_2, that is, with respect to the reference frame provided by the polygon P_2.

The angle $\omega\left(R_1 R_2^{-1}\right)$ and axis $\mathbf{e}\left(R_1 R_2^{-1}\right)$ of the relative rotation $R = R_1 R_2^{-1}$ are given by virtue of Equations (4) and (5) as

$$\omega\left(R_1 R_2^{-1}\right) = 2\arccos\left(\cos\frac{\omega_1}{2}\cos\frac{\omega_2}{2} + \sin\frac{\omega_1}{2}\sin\frac{\omega_2}{2}\,\mathbf{e}_1\cdot\mathbf{e}_2\right), \tag{13}$$

$$\mathbf{e}\left(R_1 R_2^{-1}\right) = \frac{1}{\sin\frac{\omega\left(R_1 R_2^{-1}\right)}{2}}\left(\cos\frac{\omega_2}{2}\sin\frac{\omega_1}{2}\,\mathbf{e}_1 - \cos\frac{\omega_1}{2}\sin\frac{\omega_2}{2}\,\mathbf{e}_2 - \sin\frac{\omega_1}{2}\sin\frac{\omega_2}{2}\,\mathbf{e}_1\times\mathbf{e}_2\right). \tag{14}$$

Only if the two angles of rotation are absolutely equal, that is, $\omega_2 = \pm\omega_1 = \pm\zeta$, then with Equation (6)

$$\omega\left(R_1 R_2^{-1}\right) = 2\arccos\left(\cos^2\frac{\zeta}{2} \pm \sin^2\frac{\zeta}{2}\,\mathbf{e}_1\cdot\mathbf{e}_2\right), \tag{15}$$

$$\mathbf{e}\left(R_1 R_2^{-1}\right) = \frac{1}{\sin\frac{\omega\left(R_1 R_2^{-1}\right)}{2}}\left(\sin\frac{\zeta}{2}\cos\frac{\zeta}{2}\,(\mathbf{e}_1 \mp \mathbf{e}_2) + \sin^2\frac{\zeta}{2}\,(\mp(\mathbf{e}_1\times\mathbf{e}_2))\right), \tag{16}$$

that is, the axis $\mathbf{e}\left(R_1 R_2^{-1}\right)$ is an element of the great circle spanned by either $\mathbf{e}_1 - \mathbf{e}_2$ (if $\omega_2 = \omega_1$) or $\mathbf{e}_1 + \mathbf{e}_2$ (if $\omega_2 = -\omega_1$) and $\mp(\mathbf{e}_1\times\mathbf{e}_2)$, respectively.

Since $q\left(R_2 R_1^{-1}\right) = q^*\left(R_1 R_2^{-1}\right)$, the angle and axis of $R^{-1} = R_2 R_1^{-1}$ are given as

$$\omega\left(R_2 R_1^{-1}\right) = \omega\left(R_1 R_2^{-1}\right), \tag{17}$$

$$\mathbf{e}\left(R_2 R_1^{-1}\right) = -\mathbf{e}\left(R_1 R_2^{-1}\right), \tag{18}$$

that is, the angle remains the same, and the axis flips sign. Analogously to Equation (8), an approximation of $\mathbf{e}\left(R_1 R_2^{-1}\right)$ is

$$\widehat{\mathbf{e}}\left(R_1 R_2^{-1}\right) = \frac{\omega_1\mathbf{e}_1 - \omega_2\mathbf{e}_2}{\|\omega_1\mathbf{e}_1 - \omega_2\mathbf{e}_2\|} \approx \mathbf{e}\left(R_1 R_2^{-1}\right), \tag{19}$$

that is, for sufficiently small angles ω_1 and ω_2, compare Equation (1), the normalized difference of the rotation vectors is close to the true axis $\mathbf{e}\left(R_1 R_2^{-1}\right)$ of the concatenation $R_1 R_2^{-1}$. As with respect to $R^{-1} = R_2 R_1^{-1}$ the corresponding approximation of its axis of rotation is $\widehat{\mathbf{e}}\left(R_2 R_1^{-1}\right) = -\widehat{\mathbf{e}}\left(R_1 R_2^{-1}\right)$, that is, it flips sign as the true axis.

The normalized difference of rotation vectors, Equation (19), has again and again been referred to as Euler pole of an instantaneous relative rotation obtained by simple vector addition in geoscience papers and textbooks; for example, [12]. However, by construction, it is not a Euler pole. In this communication, it is referred to as the pseudo Euler pole of the relative rotation $R_1 R_2^{-1}$ on the great circle spanned by the fixed Euler poles $\mathbf{e}_1$ and $\mathbf{e}_2$ of the rotations R_1 and R_2.

Applying Equation (7) to the relative rotation $R_1R_2^{-1}$ yields

$$\omega\left(R_1R_2^{-1}\right)\,\mathbf{e}\left(R_1R_2^{-1}\right) = \omega_{1\bar{2}}\mathbf{e}_{1\bar{2}} \approx \omega_1\,\mathbf{e}_1 - \omega_2\,\mathbf{e}_2. \tag{20}$$

4.3.3 | Circuit of relative rotations

Interchanging the roles of polygons P_1 and P_2 in a common view, the identity relationship $\left(R_1R_2^{-1}\right)\left(R_2R_1^{-1}\right) = I$ holds trivially. It generalizes for n rotations $R_1, \ldots, R_n$, $n \geq 2$, assigned one-to-one to n polygons $P_1, \ldots, P_n$ when successively considering $P_{\ell+1}$ immobile with respect to P_ℓ, $\ell = 1, \ldots, n-1$, and P_n immobile with respect to P_1 to

$$\left(R_1R_2^{-1}\right)\left(R_2R_3^{-1}\right)\,\ldots\,\left(R_{n-1}R_n^{-1}\right)\left(R_nR_1^{-1}\right) = I, \tag{21}$$

or in terms of the approximation of the corresponding multiple relative rotation vectors

$$\begin{aligned}&\boldsymbol{\omega}_{1\bar{2}} + \boldsymbol{\omega}_{2\bar{3}} + \,\ldots\, + \boldsymbol{\omega}_{n\bar{1}} = \omega_{1\bar{2}}\mathbf{e}_{1\bar{2}} + \omega_{2\bar{3}}\mathbf{e}_{2\bar{3}} + \,\ldots\, + \omega_{n\bar{1}}\mathbf{e}_{n\bar{1}}\\ &\approx (\omega_1\,\mathbf{e}_1 - \omega_2\,\mathbf{e}_2) + (\omega_2\,\mathbf{e}_2 - \omega_3\,\mathbf{e}_3) + \,\ldots\, + (\omega_n\,\mathbf{e}_n - \omega_1\,\mathbf{e}_1) = \mathbf{0},\end{aligned} \tag{22}$$

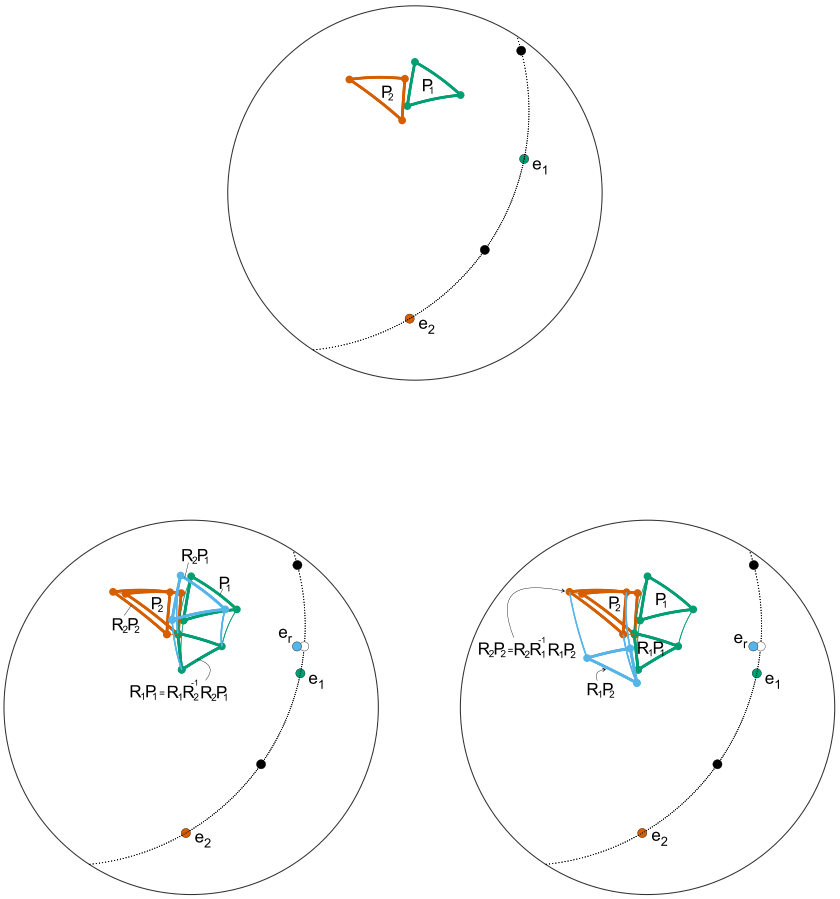

FIGURE 1 Absolute and relative circular motion on the sphere. (Top) Spherical triangle P_1 (green) and its associated fixed absolute Euler pole $\mathbf{e}_1$ (green bullet), spherical triangle P_2 (red) and its associated fixed absolute Euler pole $\mathbf{e}_2$ (red bullet), and normalized vectors (black bullets) of the sum and the difference of fixed absolute Euler poles. (Bottom left) Triangle P_1 (green) rotated for 75 Ma with rate $\varpi_1 = 0.402°/\text{Ma}$ about its fixed Euler pole $\mathbf{e}_1$ (green bullet) to R_1P_1, triangle P_2 (red) rotated for 75 Ma with rate $\varpi_2 = 0.086°/\text{Ma}$ about its fixed Euler pole $\mathbf{e}_2$ (red bullet) to R_2P_2. Considering triangle P_2 (red) to be immobile, triangle R_1P_1 (green) appears to be rotated relative to triangle R_2P_2 (red) by the relative rotation $R_1R_2^{-1}$ with ω_r about the Euler pole $\mathbf{e}_r$ (blue bullet) close to the pseudo Euler pole (black circle ∘), compare Equation (19), for sufficiently small angles. (Bottom right) Interchanging the roles of P_1 (green) and P_2 (red), triangle P_1 (green) considered to be immobile, triangle R_2P_2 (red) appears to be rotated relative to triangle R_1P_1 (green) by the relative rotation $R_2R_1^{-1}$ with $-\omega_r$ about the Euler pole $\mathbf{e}_r$ (blue bullet). [Colour figure can be viewed at wileyonlinelibrary.com]

which is referred to as plate circuit in plate tectonics when omitting the approximation, read as an equation, and expressed formally in terms of relative angular velocity vectors of tectonic plates. Here, its initial expression, Equation (21), is derived as a mathematical property of rotations and will be completed in Section 5.5.

5 | TOWARDS MODELING THE KINEMATICS OF THE MOTION OF TECTONIC PLATES

What has been sketched in Section 3 will be elaborated on here in greater detail. Throughout the following sections, spherical polygons are assumed to model the geometry of tectonic plates even though edges of spherical polygons are bound to be arcs of great circles by definition while boundaries of tectonic plates are not. Spherical polygons and tectonic plates are denoted by the same symbol P. In fact, spherical triangles are used because the focus is on illustrations of the method rather than on analyzing and modeling a specific geological setting.

5.1 | Piecewise circular motion on the sphere in terms of sequences of finite rotations

Given a sequence of strictly increasing real temporal marks $\tau_\ell, \ell = 0, 1, \ldots$, with $\tau_0 < \tau_1 < \ldots < \tau_\ell < \ldots$, assigning a unique rotation or rather orientation $R(\tau_\ell)$ to each τ_ℓ with $R(\tau_0) = I$ yields a sequence of temporally indexed rotations $R(\tau_\ell) = R(\omega(\tau_\ell), \mathbf{e}(\tau_\ell)), \ell = 0, 1, \ldots$. The corresponding rotation vectors $\boldsymbol{\omega}(\tau_\ell) = \omega(\tau_\ell)\mathbf{e}(\tau_\ell), \ell = 1, 2, \ldots$, provide the rotation rate of each individual rotation by way of the magnitude

$$\frac{\omega(\tau_\ell)}{\Delta\tau_\ell} = \|\boldsymbol{\varpi}(\tau_\ell)\|, \ell = 1, 2, \ldots,$$

of the vector

$$\boldsymbol{\varpi}(\tau_\ell) = \frac{1}{\Delta\tau_\ell}\boldsymbol{\omega}(\tau_\ell) = \frac{1}{\Delta\tau_\ell}\omega(\tau_\ell)\mathbf{e}(\tau_\ell) = \varpi(\tau_\ell)\mathbf{e}(\tau_\ell),$$

with $\Delta\tau_\ell = \tau_\ell - \tau_{\ell-1}, \ell = 1, \ldots$, of the mean angular velocity over the time interval $(\tau_{\ell-1}, \tau_\ell], \ell = 1, 2, \ldots$. Given $\mathbf{u} \in \mathbb{S}^2$, the magnitude of its corresponding mean trajectoral velocity $\mathbf{v}(\tau_\ell) = \boldsymbol{\varpi}(\tau_\ell) \times \mathbf{u}$ tangential to the arc of the circular trajectory of $\mathbf{u}$ when rotated by $R(\omega(\tau_\ell), \mathbf{e}(\tau_\ell))$ with radius $\rho = \sin\angle(\mathbf{e}(\tau_\ell), \mathbf{u})$ is

$$\|\mathbf{v}(\tau_\ell)\| = \frac{\omega(\tau_\ell)}{\Delta\tau_\ell}\rho = \frac{\omega(\tau_\ell)}{\Delta\tau_\ell}\sin\angle(\mathbf{e}(\tau_\ell), \mathbf{u}) = \|\boldsymbol{\varpi}(\tau_\ell) \times \mathbf{u}\|.$$

5.2 | Applying finite rotations successively

Given a spherical polygon P, the expression

$$R(\tau_\ell)R(\tau_{\ell-1}) \ldots R(\tau_2)R(\tau_1)P$$

can be read in two different ways, either

$$R(\tau_\ell)\left(R(\tau_{\ell-1}) \ldots (R(\tau_2)(R(\tau_1)P))\right) = P^{(\ell)}, \ell = 1, 2, \ldots, \tag{23}$$

with $R(\tau_\ell)$ being applied to the immediately preceding rotational state $P^{(\ell-1)}, \ell = 1, 2, \ldots$, of the initial polygon P, that is, with

$$P^{(0)} = R(\tau_0)P, P^{(\ell)} = R(\tau_\ell)P^{(\ell-1)}, \ell = 1, 2, \ldots,$$

or

$$\left(R(\tau_\ell)R(\tau_{\ell-1}) \ldots R(\tau_2)R(\tau_1)\right)P = R^{(\ell)}P, \ell = 1, 2, \ldots, \tag{24}$$

where $R^{(\ell)}$ denotes the successive concatenation of the first ℓ elements of the sequence $R(\tau_\ell), \ell = 1, 2, \dots$, being applied to the initial polygon P for all $\ell = 1, 2, \dots$. The sequence of Equation (23) will be referred to as sequence of consecutive incremental finite rotations, and the sequence of Equation (24) will be referred to as accumulated total rotation by successive concatenation of incremental finite rotations.

Since in the strict mathematical sense a rotation is an instantaneous transformation of a given to a transformed orientation of an object, compare Section 2, the final orientation of the polygon is of course the same for both models,

$$P^{(\ell)} = R(\tau_\ell)P^{(\ell-1)} = \left(R(\tau_\ell)R^{(\ell-1)}\right)P = R^{(\ell)}P, \ell = 1, 2, \dots .$$

However, thinking of a rotation as a circular motion continuously changing the given initial to a transformed final orientation of an object, the trajectories of a vertex of P to the corresponding vertex of $P^{(\ell)}, \ell = 2, 3, \dots$, are generally different for the two models. Applying the model of consecutive incremental rotations, Equation (23), the trajectory is continuously composed of arcs of different circles. If, on the other hand, the model of successive concatenation, Equation (24), is being applied, the trajectory comprises an arc of a unique circle.

Next, both models will be applied to the "three-plate problem" of plate tectonics in the following paragraphs.

5.2.1 | Piecewise circular motion on the sphere by sequences of incremental finite rotations

Two initial plates P_1 and P_2 are rotated incrementally, that is,

$$P_i^{(0)} = R_i(\tau_0)P_i, P_i^{(\ell)} = R_i(\tau_\ell)P_i^{(\ell-1)}, i = 1, 2,\ \ell = 1, 2, \dots , \tag{25}$$

with $R_i(\tau_\ell) = R(\omega_i(\tau_\ell), \mathbf{e}_i(\tau_\ell)), i = 1, 2,\ \ell = 1, 2, \dots$, with respect to a third plate considered to be fixed thus providing a fixed reference system. Then, the paths of the absolute motion of the two plates, that is, the trajectories of their vertices, are continuously composed consecutive circular arcs according to $R\left(\omega_i(\tau_\ell), \mathbf{e}_i(\tau_\ell)\right)$ of sizes $\omega_i(\tau_\ell)$ joint at τ_ℓ. If the Euler poles are stationary, that is, $\mathbf{e}_i(\tau_\ell) = \mathbf{e}_i, i = 1, 2,\ \ell = 1, 2, \dots$, then the entire paths from $P_i^{(0)}$ to $P_i^{(\ell)}$ are arcs of size $\sum_\ell \omega_i(\tau_\ell)$ of unique circles.

Applying Equations (11) and (12), the path of the relative motion of $P_1^{(\ell-1)}$ with respect to $P_2^{(\ell)}$ considered to be immobile is given by

$$\begin{aligned}\Delta R(\tau_\ell) &= R_1(\tau_\ell)(R_2(\tau_\ell))^{-1}\\ &= R\left(\omega_1(\tau_\ell), \mathbf{e}_1(\tau_\ell)\right)\ \left(R\left(\omega_2(\tau_\ell), \mathbf{e}_2(\tau_\ell)\right)\right)^{-1}, \ell = 1, 2, \dots ,\end{aligned}$$

applied to $P_2^{(\ell)}$, and the path of the relative motion of polygon $P_2^{(\ell-1)}$ as observed from polygon $P_1^{(\ell)}$ considered to be immobile is given by

$$\begin{aligned}(\Delta R(\tau_\ell))^{-1} &= R_2(\tau_\ell)(R_1(\tau_\ell))^{-1}\\ &= R\left(\omega_2(\tau_\ell), \mathbf{e}_2(\tau_\ell)\right)\left(R\left(\omega_1(\tau_\ell), \mathbf{e}_1(\tau_\ell)\right)\right)^{-1}, \ell = 1, 2, \dots ,\end{aligned}$$

applied to $P_1^{(\ell)}$.

Four consecutive steps of absolute and relative incrementally piecewise circular motion on the sphere are depicted in Figure 2.

The angle and axis of $\Delta R(\tau_\ell)$ and $(\Delta R(\tau_\ell))^{-1}$, respectively, are given by application of Equations (13) and (14) and Equations (17) and (18), respectively. If $\omega_i(\tau_\ell), i = 1, 2$, are assumed to be sufficiently small, compare Equation (1), then the approximation Equation (19) applies and

$$\widehat{\mathbf{e}}\left(\Delta R(\tau_\ell)\right) = \frac{\omega_1(\tau_\ell)\mathbf{e}_1(\tau_\ell) - \omega_2(\tau_\ell)\mathbf{e}_2(\tau_\ell)}{\|\omega_1(\tau_\ell)\mathbf{e}_1(\tau_\ell) - \omega_2(\tau_\ell)\mathbf{e}_2(\tau_\ell)\|} \approx \mathbf{e}\left(\Delta R(\tau_\ell)\right).$$

In the most simple case assuming stationary Euler poles $\mathbf{e}_i(\tau_\ell) = \mathbf{e}_i$ and sufficiently small constant angles $\omega_i(\tau_\ell) = \omega_i, i = 1, 2$, for example, constant rates $\varpi_i, i = 1, 2$, and unique time lags $\Delta\tau = \tau_\ell - \tau_{\ell-1}, \ell = 1, 2, \dots$ such that $\omega_i = \Delta\tau\varpi_i, i = 1, 2$, are sufficiently small, the pseudo Euler pole $\widehat{\mathbf{e}}(\Delta R(\tau_\ell))$ of the incremental relative rotation is seen to be stationary as

$$\widehat{\mathbf{e}}\left(\Delta R(\tau_\ell)\right) = \frac{\Delta\tau\varpi_1\mathbf{e}_1 - \Delta\tau\varpi_2\mathbf{e}_2}{\|\Delta\tau\varpi_1\mathbf{e}_1 - \Delta\tau\varpi_2\mathbf{e}_2\|}$$

becomes independent of τ_ℓ.

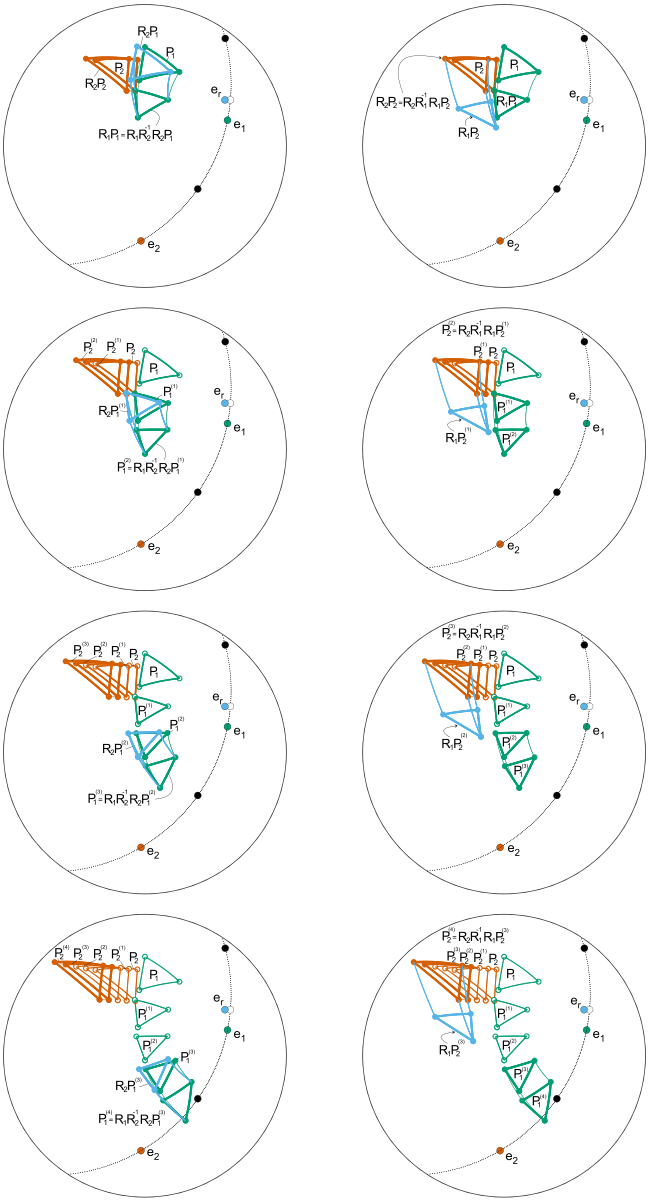

FIGURE 2 Four consecutive steps of absolute and relative incrementally piecewise circular motion on the sphere. (Rows 1 to 4, left column) Triangle P_1 (green) successively incrementally rotated by $\omega_1 = 0.402°$ about its fixed Euler pole $\mathbf{e}_1$ (green bullet) to $P_1^{(\ell)}, \ell = 0, \ldots, 4$, (Equation 25), triangle P_2 (red) successively rotated by $\omega_2 = 0.086°$ about its fixed Euler pole $\mathbf{e}_2$ (red bullet) to $P_2^{(\ell)}, \ell = 0, \ldots, 4$, considering triangle $P_2^{(\ell)}$ (red) to be immobile, triangle $P_1^{(\ell)}$ (green) appears to be rotated relative to triangle $P_2^{(\ell)}, \ell = 1, \ldots, 4$, (red) by the relative rotation $R_1 R_2^{-1}$ about the Euler pole $\mathbf{e}_r$ (blue bullet) close to the pseudo Euler pole (black circle ∘), compare Equation (19), for sufficiently small angles. (Rows 1 to 4, right column) Interchanging the roles of P_1 (green) and P_2 (red), triangle $P_1^{(\ell)}$ (green) considered to be immobile, triangle $P_2^{(\ell)}$ (red) appears to be rotated relatively to triangle $P_1^{(\ell)}, \ell = 1, \ldots, 4$, (green) by the relative rotation $R_2 R_1^{-1}$ about the Euler pole $\mathbf{e}_r$ (blue bullet). [Colour figure can be viewed at wileyonlinelibrary.com]

5.2.2 | Piecewise circular motion on the sphere by accumulating successive concatenations of finite rotations

Successive concatenations of rotations of two sequences of temporally indexed rotations provide another simple model to resolve the three-plate problem in terms of accumulated total absolute and relative motion. The findings of Sections 4.2 and 4.3 immediately apply to determine the paths of the absolute motion of the two plates, that is, the trajectories of their vertices, as well as the path of the relative motion of P_1 with respect to P_2 if considered to be immobile, and its corresponding migrating Euler pole (MEP).

The initial two plates $P_i, i = 1, 2$, are subject to rotations $R\left(\Omega_i(\tau_\ell), \mathbf{E}_i(\tau_\ell)\right)$ such that

$$R_i^{(\ell)} P_i = R\left(\Omega_i(\tau_\ell), \mathbf{E}_i(\tau_\ell)\right) P_i = P_i^{(\ell)}, i = 1, 2,\ \ell = 1, 2, \ldots, \tag{26}$$

resulting from successive concatenations of rotations $R(\omega_i(\tau_j), \mathbf{e}_i(\tau_j)), j = 1, \ldots, \ell$, that is,

$$\begin{aligned} R\left(\Omega_i(\tau_\ell), \mathbf{E}_i(\tau_\ell)\right) = R\left(\omega_i(\tau_\ell), \mathbf{e}_i(\tau_\ell)\right) R\left(\omega_i(\tau_{\ell-1}), \mathbf{e}_i(\tau_{\ell-1})\right) \ \ldots \\ \ldots\ R\left(\omega_i(\tau_1), \mathbf{e}_i(\tau_1)\right), i = 1, 2,\ \ell = 1, 2, \ldots. \end{aligned} \tag{27}$$

The trajectories of the vertices of P_i to the corresponding vertices of $P_i^{(\ell)}$ are described by Equation (26), that is, by the accumulated total change of the rotational state at time τ_ℓ.

Considering P_2 to be immobile, the angle $\omega_{\mathrm{MEP}}(\tau_\ell)$ and axis $\mathbf{e}_{\mathrm{MEP}}(\tau_\ell)$ of the relative rotation

$$R = R\left(\omega_{\mathrm{MEP}}(\tau_\ell), \mathbf{e}_{\mathrm{MEP}}(\tau_\ell)\right) = R\left(\Omega_1(\tau_\ell), \mathbf{E}_1(\tau_\ell)\right)\left(R\left(\Omega_2(\tau_\ell), \mathbf{E}_2(\tau_\ell)\right)\right)^{-1}$$

are given by virtue of Equations (13) and (14) as

$$\omega_{\mathrm{MEP}}(\tau_\ell) = 2 \arccos\left(\cos\frac{\Omega_1(\tau_\ell)}{2}\cos\frac{\Omega_2(\tau_\ell)}{2} + \sin\frac{\Omega_1(\tau_\ell)}{2}\sin\frac{\Omega_2(\tau_\ell)}{2}\boldsymbol{E}_1(\tau_\ell)\cdot\boldsymbol{E}_2(\tau_\ell)\right) \tag{28}$$

$$\begin{aligned} \mathbf{e}_{\mathrm{MEP}}(\tau_\ell) = \frac{1}{\sin\frac{\omega_{\mathrm{MEP}}(\tau_\ell)}{2}}\Bigg(\cos\frac{\Omega_2(\tau_\ell)}{2}\sin\frac{\Omega_1(\tau_\ell)}{2}\boldsymbol{E}_1(\tau_\ell) - \cos\frac{\Omega_1(\tau_\ell)}{2}\sin\frac{\Omega_2(\tau_\ell)}{2}\boldsymbol{E}_2(\tau_\ell) \\ - \sin\frac{\Omega_1(\tau_\ell)}{2}\sin\frac{\Omega_2(\tau_\ell)}{2}\boldsymbol{E}_1(\tau_\ell)\times\boldsymbol{E}_2(\tau_\ell)\Bigg). \end{aligned} \tag{29}$$

Assuming stationary absolute Euler poles $\mathbf{e}_i(\tau_\ell) = \mathbf{e}_i, i = 1, 2$, for all $\ell = 1, 2, \ldots$, resulting in $\boldsymbol{E}_i(\tau_\ell) = \boldsymbol{E}_i = \mathbf{e}_i$, or assuming constant rates $\varpi_i(\tau_\ell) = \varpi_i, i = 1, 2$, resulting in $\Omega_i(\tau_\ell) = \sum_{j=1}^{\ell}\Delta\tau_j\varpi_i$, $i = 1, 2$, for all $\ell = 1, 2, \ldots$, would simplify the model. As known from Equation (16), the axes $\mathbf{e}_{\mathrm{MEP}}(\tau_\ell), \ell = 1, 2, \ldots$, of successive accumulated total relative rotations migrate along a great circle if the absolute Euler poles $\mathbf{e}_i$ are stationary and the rates are absolutely equal, that is, $|\varpi_1| = |\varpi_2|$. Otherwise, and contrary to [13], the path of the migrating Euler pole is not generally a small circle centered at one of the absolute Euler poles.

Absolute and relative accumulated total piecewise circular motion after four steps, that is, after 300 Ma, is shown in Figure 3, confirming by the way that the migrating Euler pole does not generally move along a small circle.

The approximation

$$\widehat{\mathbf{e}}_{\mathrm{MEP}}(\tau_\ell) = \frac{\Omega_1(\tau_\ell)\mathbf{E}_1(\tau_\ell) - \Omega_2(\tau_\ell)\mathbf{E}_2(\tau_\ell)}{\|\Omega_1(\tau_\ell)\mathbf{E}_1(\tau_\ell) - \Omega_2(\tau_\ell)\mathbf{E}_2(\tau_\ell)\|} \approx \mathbf{e}_{\mathrm{MEP}}(\tau_\ell) \tag{30}$$

holds if $\Omega_i(\tau_\ell), i = 1, 2$, are sufficiently small, compare Equation (19). Since constant rates $\varpi_i(\tau_\ell) = \varpi_i$ result in $\Omega_i(\tau_\ell) = \sum_{j=1}^{\ell}\Delta\tau_j\varpi_i, i = 1, 2$, for all $\ell = 1, 2, \ldots$, Equation (30) simplifies to

$$\begin{aligned} \widehat{\mathbf{e}}_{\mathrm{MEP}} &= \frac{\sum_{j=1}^{\ell}\Delta\tau_j\varpi_1\mathbf{E}_1(\tau_\ell) - \sum_{j=1}^{\ell}\Delta\tau_j\varpi_2\mathbf{E}_2(\tau_\ell)}{\|\sum_{j=1}^{\ell}\Delta\tau_j\varpi_2\mathbf{E}_1(\tau_\ell) - \sum_{j=1}^{\ell}\Delta\tau_j\varpi_2\mathbf{E}_2(\tau_\ell)\|} \\ &= \frac{\varpi_1\mathbf{E}_1(\tau_\ell) - \varpi_2\mathbf{E}_2(\tau_\ell)}{\|\varpi_1\mathbf{E}_1(\tau_\ell) - \varpi_2\mathbf{E}_2(\tau_\ell)\|}, \end{aligned} \tag{31}$$

revealing that with the additional assumption of stationary Euler poles $\boldsymbol{E}_i(\tau_\ell) = \boldsymbol{E}_i = \mathbf{e}_i,\ i = 1, 2$, the pseudo Euler pole $\widehat{\mathbf{e}}_{\mathrm{MEP}}$ is stationary. Depending on the rates ϖ_i and the time lags τ_ℓ such that $\sum_{j=1}^{\ell}\Delta\tau_j\varpi_i$ are sufficiently small, it may be expected that

$$\widehat{\mathbf{e}}_{\mathrm{MEP}} \approx \mathbf{e}_{\mathrm{MEP}}(\tau_\ell), \ell = 1, \ldots, L_0, \tag{32}$$

that is, that the stationary pseudo Euler pole $\widehat{\mathbf{e}}_{\mathrm{MEP}}$ is close to the first few $\mathbf{e}_{\mathrm{MEP}}(\tau_\ell)$ with $\ell = 1, \ldots, L_0$ only. Otherwise, Equation (31) provides a poor approximation.

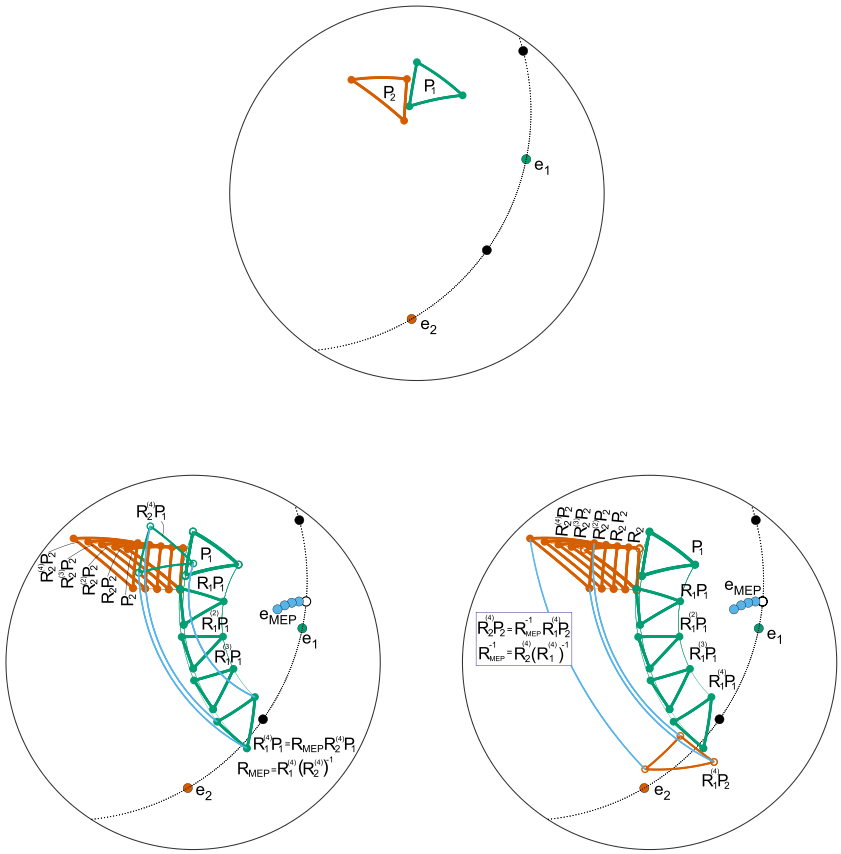

FIGURE 3 Absolute and relative accumulated total piecewise circular motion on the sphere after four steps, that is, after 300 Ma. (Top) Spherical triangle P_1 (green) and its associated fixed absolute Euler pole $\mathbf{e}_1$ (green bullet), spherical triangle P_2 (red) and its associated fixed absolute Euler pole $\mathbf{e}_2$ (red bullet), normalized vectors (black bullets) of the sum and the difference of fixed absolute Euler poles, pseudo Euler pole (Equation 19) (black circle ∘) for sufficiently small angles of rotation, and unit vector of the sum of rotation vectors $\omega_1\mathbf{e}_1 + \omega_2\mathbf{e}_2$ (black circle ∘) which is fixed as the ratio of rates $\tau\omega_1/\tau\omega_2 = \omega_1/\omega_2$ remains constant through time. (Bottom left) Triangle P_1 (green) successively rotated with stepsize given by multiples (75) of rate $\varpi_1 = 0.402°/\text{Ma}$ about its fixed Euler pole $\mathbf{e}_1$ (green bullet) to $R_1^{(\ell)}P_1, \ell = 1, \ldots, 4$ (Equation 26), triangle P_2 (red) successively rotated with stepsize given by multiples (75) of rate $\varpi_2 = 0.086°/\text{Ma}$ about its fixed Euler pole $\mathbf{e}_2$ (red bullet) to $R_2^{(\ell)}P_2, \ell = 1, \ldots, 4$, considering triangle $R_2^{(\ell)}P_2$ (red) to be immobile, triangle $R_1^{(\ell)}P_1$ (green) appears to be rotated relative to triangle $R^{(\ell)}P_2$ (red) by the relative rotation $R_{\text{MEP}} = R_1^{(\ell)}(R_2^{(\ell)})^{-1}, \ell = 1, \ldots, 4$, about the migrating Euler pole $\mathbf{e}_{\text{MEP}}$ (blue bullets). (Bottom right) Interchanging the roles of P_1 (green) and P_2 (red), triangle $R_1^{(\ell)}P_1$ (green) considered to be immobile, triangle $R_2^{(\ell)}P_2$ (red) appears to be rotated relatively to triangle $R^{(\ell)}P_1$ (green) by the relative rotation $(R_{\text{MEP}})^{-1} = R_2^{(\ell)}\left(R_1^{(\ell)}\right)^{-1}, \ell = 1, \ldots, 4$, about the migrating Euler pole $\mathbf{e}_{\text{MEP}}$ (blue bullets). [Colour figure can be viewed at wileyonlinelibrary.com]

5.2.3 | Features of accumulated total rotations

It might be geologically tempting to hypothesize simple relationships linking a sequence of accumulated total to their incremental rotations in terms of invariant geometrical or topological features. For instance, if polygon P_1 is considered to be immobile, compare Figures 2 and 3, the migrating relative Euler pole $\mathbf{e}_{\text{MEP}}^{(\ell)}$ might be imagined to be immobile with respect to $R_1^{(\ell)}P_2$ being rotated to $R_2^{(\ell)}P_2$ by the relative rotation $R_2^{(\ell)}\left(R_1^{(\ell)}\right)^{-1}$. However, simple computations summarized in Table 1 and a closer look, Figure 4, reveal that the angle between the Euler pole $\mathbf{e}_{\text{MEP}}^{(\ell)}$ and a given vertex $\mathbf{v}^{(\ell)}$ of $R_1^{(\ell)}P_2, \ell = 1, \ldots, 4$, is not constant.

5.3 | Continuous rotation in terms of time-dependent quaternion and continuous circular motion on the sphere in terms of its temporal derivative

Angular displacement and both angular and trajectoral velocity of a transient rotation are derived as functions of time in terms of temporal derivatives of transient quaternions with special emphasis on the angle-axis parametrization of rotations, unlike [14, pp. 56–59] applying quaternion and (3×3) matrix notation.

TABLE 1 Features of accumulated total rotations $R(\varpi_1 t, \mathbf{e}_1)$ and $R(\varpi_2 t, \mathbf{e}_2)$ about fixed Euler poles $\mathbf{e}_1$ and $\mathbf{e}_2$, respectively, and their accumulated total relative rotation $R(\varpi_2 t, \mathbf{e}_2)(R(\varpi_1 t, \mathbf{e}_1))^{-1}$.

t (Ma)	$\omega_1 = \varpi_1 t$ (°)	$\omega_2 = \varpi_2 t$ (°)	ω_{MEP} (°)	η (°)	θ (°)
75	30.2	6.4	31.5	87.0	3.0
150	60.4	12.9	62.9	90.0	3.2
225	90.5	19.3	94.1	93.3	3.4
300	120.7	25.7	125.0	97.0	3.8

Note: col 1: t time mark; col 2: $\omega_1 = \varpi_1 t$ cumulative angle of rotation about fixed Euler pole $\mathbf{e}_1$ with $\varpi_1 = 0.402$ (°/Ma); col 3: $\omega_2 = \varpi_2 t$ cumulative angle of rotation about fixed Euler pole $\mathbf{e}_2$ with $\varpi_2 = 0.086$ (°/Ma); col 4: ω_{MEP} cumulative angle of rotation about migrating Euler pole $\mathbf{e}_{\text{MEP}}$; col 5: $\eta = \angle(\mathbf{e}_{\text{MEP}}, \mathbf{v})$ spherical distance (along great circle) between successive migrating relative Euler pole $\mathbf{e}_{\text{MEP}}$ and given edge $\mathbf{v}$ of polygon being rotated; col 6: $\theta = \angle(\mathbf{e}_{\text{MEP}}(t), \mathbf{e}_{\text{MEP}}(t - \Delta t))$, $\Delta t = 75$ Ma, spherical distance (along great circle) between successive relative Euler poles $\mathbf{e}_{\text{MEP}}$ migrating along their path which is not a circle.

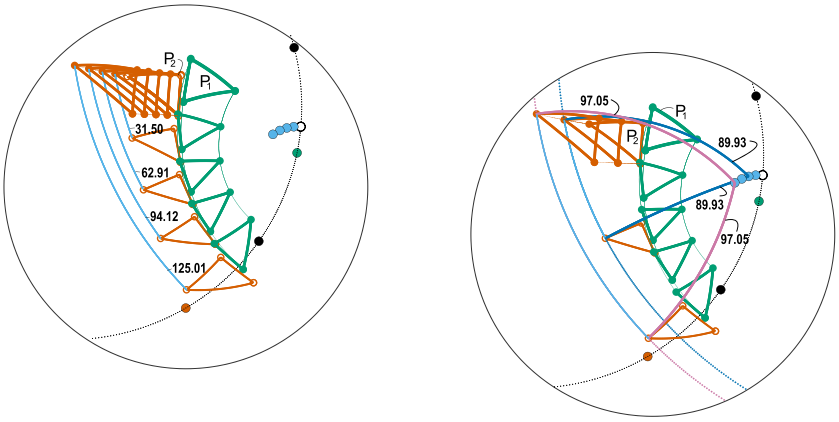

FIGURE 4 Features of accumulated total rotations $R(\varpi_1 t_\ell, \mathbf{e}_1)$ and $R(\varpi_2 t_\ell, \mathbf{e}_2)$ about fixed Euler poles $\mathbf{e}_1$ (green bullet) and $\mathbf{e}_2$ (red bullet), respectively, with $\varpi_1 = 0.402$ (°/Ma), $\varpi_2 = 0.086$ (°/Ma), and $t_\ell = \ell$ 75 (Ma), $\ell = 1, \ldots, 4$, and their accumulated total relative rotation $R(\varpi_2 t, \mathbf{e}_2)(R(\varpi_1 t, \mathbf{e}_1))^{-1}$ about migrating Euler poles $\mathbf{e}_{\text{MEP}}^{(\ell)}$, $\ell = 1, \ldots, 4$, (blue bullets). (Left) The trajectories of a given vertex $\mathbf{v}^{(\ell)}$ of $R_2^{(\ell)}\left(R_1^{(\ell)}\right)^{-1} P_2$ rotating about the relative Euler pole $\mathbf{e}_{\text{MEP}}^{(\ell)}$, $\ell = 1, \ldots, 4$, are not arcs of concentric circles, because their centers are the migrating Euler poles. (Right) The angles of a given vertex $\mathbf{v}^{(\ell)}$ of $R_2^{(\ell)}\left(R_1^{(\ell)}\right)^{-1} P_2$ and the axis of its rotation $R_2^{(\ell)}\left(R_1^{(\ell)}\right)^{-1}$, $\ell = 1, \ldots, 4$, the migrating Euler pole, are not constant. [Colour figure can be viewed at wileyonlinelibrary.com]

Considering a transient rotation $R(\omega(t), \mathbf{e}(t))$ in terms of quaternions

$$q(t) = \cos\frac{\omega(t)}{2} + \mathbf{e}(t)\sin\frac{\omega(t)}{2}, t \in \mathbb{R},$$

its temporal derivative is given by

$$\frac{d}{dt}q(t) = \frac{d}{dt}q_0(t) + \frac{d}{dt}\mathbf{q}(t),$$

that is, explicitly

$$\dot{q}(t) = -\frac{1}{2}\dot{\omega}(t)\sin\frac{\omega(t)}{2} + \frac{1}{2}\dot{\omega}(t)\cos\frac{\omega(t)}{2}\mathbf{e}(t) + \sin\frac{\omega(t)}{2}\dot{\mathbf{e}}(t), \tag{33}$$

where the derivative with respect to t is denoted by a dot on top of the symbol. Then, the trajectory of the pure quaternion, that is, vector $\mathbf{u}_0$, under the rotation specified by $q(t)$ is

$$\mathbf{u}(t) = q(t) \circ \mathbf{u}_0 \circ q^*(t), \tag{34}$$

and its instantaneous trajectoral velocity by

$$\begin{aligned}\mathbf{v}(t) = \dot{\mathbf{u}}(t) &= \dot{q}(t) \circ \mathbf{u}_0 \circ q^*(t) + q(t) \circ \mathbf{u}_0 \circ \dot{q^*}(t) \\ &= \dot{q}(t) \circ \mathbf{u}_0 \circ q^*(t) + q(t) \circ \mathbf{u}_0 \circ \dot{q}^*(t),\end{aligned} \tag{35}$$

applying $\frac{d}{dt}q^*(t) = \left(\frac{d}{dt}q(t)\right)^*$. Replacing $\mathbf{u}_0$ in Equation (35) with $q^*(t)\mathbf{u}(t)q(t)$ from Equation (34) gives

$$\begin{aligned}\mathbf{v}(t) &= \dot{q}(t) \circ q^*(t) \circ \mathbf{u}(t) + \mathbf{u}(t) \circ q(t) \circ \dot{q}^*(t) \\ &= \dot{q}(t) \circ q^*(t) \circ \mathbf{u}(t) + \mathbf{u}(t) \circ (\dot{q}(t) \circ q^*(t))^*.\end{aligned} \tag{36}$$

5.3.1 | Transient angle and stationary axis of rotation

In the special case that the axis of rotation is assumed to be stationary, Equation (33) simplifies to

$$\dot{q}(t) = -\frac{1}{2}\dot{\omega}(t)\sin\frac{\omega(t)}{2} + \frac{1}{2}\dot{\omega}(t)\cos\frac{\omega(t)}{2}\mathbf{e}$$

and yields

$$\begin{aligned}\dot{q}(t) \circ q^*(t) &= \frac{1}{2}\dot{\omega}(t)\left(-\sin\frac{\omega(t)}{2} + \mathbf{e}\cos\frac{\omega(t)}{2}\right) \circ \left(\cos\frac{\omega(t)}{2} - \mathbf{e}\sin\frac{\omega(t)}{2}\right) \\ &= \frac{1}{2}\dot{\omega}(t)\mathbf{e}.\end{aligned}$$

The pure quaternion $2\dot{q}(t) \circ q^*(t)$ is referred to as the vector of the instantaneous angular velocity

$$\dot{\boldsymbol{\omega}}(t) = \dot{\omega}(t)\mathbf{e} = 2\dot{q}(t) \circ q^*(t), \tag{37}$$

with magnitude $\|\dot{\boldsymbol{\omega}}(t)\| = |\dot{\omega}(t)|$. Then, the instantaneous trajectoral velocity is

$$\mathbf{v}(t) = \frac{1}{2}\left(\dot{\boldsymbol{\omega}}(t) \circ \mathbf{u}(t) - \mathbf{u}(t) \circ \dot{\boldsymbol{\omega}}(t)\right) = \dot{\boldsymbol{\omega}}(t) \times \mathbf{u}(t), \tag{38}$$

$$\|\mathbf{v}(t)\| = |\dot{\omega}(t)| \sin \angle(\mathbf{e}, \mathbf{u}(t)), \tag{39}$$

with instantaneous angular rate $\dot{\omega}(t) = \frac{d}{dt}\omega(t)$. If $\dot{\omega}(t) = \text{const}$, then the motion is uniform, $\omega(t) = ct$ and $\dot{\boldsymbol{\omega}}(t) = c\mathbf{e}$.

5.3.2 | Transient angle and axis of rotation

The equation of departure is Equation (36). Since

$$q(t) \circ q^*(t) = 1$$

implies

$$\dot{q}(t) \circ q^*(t) + q(t) \circ \dot{q}^*(t) = \dot{q}(t) \circ q^*(t) + (\dot{q}(t) \circ q^*(t))^* = 0, \tag{40}$$

it follows that $\dot{q}(t) \circ q^*(t)$ is a pure quaternion, that is, a vector. It satisfies

$$\dot{q}(t) \circ q^*(t) = \frac{1}{2}\dot{\boldsymbol{\omega}}(t).$$

Then, with Equation (40)

$$\dot{\boldsymbol{\omega}}(t) = 2\dot{q}(t) \circ q^*(t) = -2q(t) \circ \dot{q}^*(t), \tag{41}$$

and as before, compare Equation (38), the vector of the instantaneous trajectoral velocity is

$$\mathbf{v}(t) = \frac{1}{2}\left(\dot{\boldsymbol{\omega}}(t) \circ \mathbf{u}(t) - \mathbf{u}(t) \circ \dot{\boldsymbol{\omega}}(t)\right) = \dot{\boldsymbol{\omega}}(t) \times \mathbf{u}(t). \tag{42}$$

To complete the short outlook of Section 3.2, given angle and axis of rotation as continuous function of time, Equations (27) and (26) and Equations (28) and (29) require little revision only dropping successive concatenation and replacing $\Omega_{(\tau_\ell)}, \mathbf{E}(\tau_\ell), \ell = 1, 2, \ldots$, depending on discrete time steps $\tau_\ell, \ell = 1, 2, \ldots$, by continuous functions $\omega(t), \mathbf{e}(t)$ to allow to compute location, absolute and relative rotation (orientation), angular and trajectoral velocity of the polygons being rotated, and more features of the motion on the sphere for any given time.

5.4 | Migrating Euler pole

For example, for a general transient view of the model of accumulated total absolute and relative motion of two plates and their migrating relative Euler pole the notation is slightly changed to adapt to the continuous time dependence.

Then, the temporal derivative of the transient relative rotation $q_1(t)q_2^*(t)$ (considering P_2 fixed) is

$$\frac{d}{dt}\left(q_1(t) \circ q_2^*(t)\right) = \dot{q}_1(t) \circ q_2^*(t) + q_1(t) \circ \dot{q}_2^*(t),$$

and the relative instantaneous angular velocity is

$$\begin{aligned}
\frac{1}{2}\dot{\boldsymbol{\omega}}\left[R_1R_2^{-1}\right](t) &= \left(\frac{d}{dt}q_1(t) \circ q_2^*(t)\right) \circ \left(q_1(t) \circ q_2^*(t)\right)^* \\
&= \left(\dot{q}_1(t) \circ q_2^*(t) + q_1(t) \circ \dot{q}_2^*(t)\right) \circ \left(q_2(t) \circ q_1^*(t)\right) \\
&= \dot{q}_1(t) \circ q_1^*(t) + q_1(t) \circ \left(\dot{q}_2^*(t) \circ q_2(t)\right) \circ q_1^*(t) \\
&= \frac{1}{2}\dot{\boldsymbol{\omega}}_1(t) + q_1(t) \circ \left(\dot{q}_2^*(t) \circ q_2(t)\right) \circ q_1^*(t).
\end{aligned}$$

For a complementary view, the focus is separately on the transient relative angle of rotation and its derivative, the scalar angular velocity, and on the transient relative axis of rotation and its derivative, the path of the migrating Euler pole. To this end Equations (13) and (14) are rewritten in terms of time-dependent variables:

$$\omega\left[R_1R_2^{-1}\right](t) = 2\arccos\left(\cos\frac{\omega_1(t)}{2}\cos\frac{\omega_2(t)}{2} + \sin\frac{\omega_1(t)}{2}\sin\frac{\omega_2(t)}{2}\,\mathbf{e}_1(t) \cdot \mathbf{e}_2(t)\right), \tag{43}$$

$$\mathbf{e}\left[R_1R_2^{-1}\right](t) = \frac{1}{\sin\frac{\omega\left[R_1R_2^{-1}\right](t)}{2}}\left(\cos\frac{\omega_2(t)}{2}\sin\frac{\omega_1(t)}{2}\,\mathbf{e}_1(t) - \cos\frac{\omega_1(t)}{2}\sin\frac{\omega_2(t)}{2}\,\mathbf{e}_2(t) - \sin\frac{\omega_1(t)}{2}\sin\frac{\omega_2(t)}{2}\,\mathbf{e}_1(t) \times \mathbf{e}_2(t)\right). \tag{44}$$

To begin with the most simple case to accomplish instructive results, the individual Euler poles $\mathbf{e}_i, i = 1, 2$, are assumed to be stationary, that is, $\mathbf{e}_i(t) = \mathbf{e}_i, i = 1, 2$, and the rates $\dot{\omega}_i(t) = \varpi_i, i = 1, 2$, are assumed to be constant, that is, $\omega_i(t) = \varpi_i t, i = 1, 2$.

5.4.1 | Transient rotation rate with respect to migrating Euler pole

From Equation (43) and

$$\frac{d}{dt}\cos\frac{\omega\left[R_1R_2^{-1}\right](t)}{2} = -\frac{1}{2}\sin\frac{\omega\left[R_1R_2^{-1}\right](t)}{2}\,\dot{\omega}\left[R_1R_2^{-1}\right](t),$$

$\dot{\omega}\left[R_1R_2^{-1}\right](t)$ satisfies

$$\begin{aligned}\dot{\omega}\left[R_1R_2^{-1}\right](t) &= -\frac{2}{\sin\frac{\omega\left[R_1R_2^{-1}\right](t)}{2}}\frac{d}{dt}\left(\cos\frac{\omega_1(t)}{2}\cos\frac{\omega_2(t)}{2}+\sin\frac{\omega_1(t)}{2}\sin\frac{\omega_2(t)}{2}\mathbf{e}_1\cdot\mathbf{e}_2\right)\\ &= \frac{2}{\sin\frac{\omega\left[R_1R_2^{-1}\right](t)}{2}}\left(\frac{\varpi_1}{2}\sin\frac{\varpi_1 t}{2}\cos\frac{\varpi_2 t}{2}+\frac{\varpi_2}{2}\sin\frac{\varpi_2 t}{2}\cos\frac{\varpi_1 t}{2}\right.\\ &\quad\left.-\mathbf{e}_1\cdot\mathbf{e}_2\left(\frac{\varpi_1}{2}\cos\frac{\varpi_1 t}{2}\sin\frac{\varpi_2 t}{2}+\frac{\varpi_2}{2}\cos\frac{\varpi_2 t}{2}\sin\frac{\varpi_1 t}{2}\right)\right),\end{aligned} \tag{45}$$

and in the special case of absolutely equal rates $|\varpi_1| = |\varpi_2|$

$$\dot{\omega}\left[R_1R_2^{-1}\right](t) = \frac{2}{\sin\frac{\omega\left[R_1R_2^{-1}\right](t)}{2}}\left(1\mp\mathbf{e}_1\cdot\mathbf{e}_2\right)\ \bar{\zeta}\sin\frac{\bar{\zeta}t}{2}\cos\frac{\bar{\zeta}t}{2}.$$

5.4.2 | Trajectory of migrating Euler pole

To determine the temporal derivative of the migrating Euler pole $\mathbf{e}\left[R_1R_2^{-1}\right](t)$ of Equation (44) recall that for any unit vector $\mathbf{e}(t)\in\mathbb{S}^2$ $\mathbf{e}(t)\cdot\mathbf{e}(t)=1$, thus

$$0 = \frac{d}{dt}\left(\mathbf{e}(t)\cdot\mathbf{e}(t)\right) = 2\dot{\mathbf{e}}(t)\cdot\mathbf{e}(t),$$

that is, $\mathbf{e}(t)$ and its temporal derivative $\dot{\mathbf{e}}(t)$ are orthogonal.

Using the same assumptions as in Section 5.4.1, Equation (44) may be rewritten as

$$\mathbf{e}\left[R_1R_2^{-1}\right](t) = \varphi(t)\mathbf{q}(t),$$

with

$$\begin{aligned}\varphi(t) &= \frac{1}{\|\mathbf{q}(t)\|} = \frac{1}{\sin\frac{\omega\left[R_1R_2^{-1}\right](t)}{2}},\\ \mathbf{q}(t) &= \cos\frac{\omega_2(t)}{2}\sin\frac{\omega_1(t)}{2}\mathbf{e}_1-\cos\frac{\omega_1(t)}{2}\sin\frac{\omega_2(t)}{2}\mathbf{e}_2-\sin\frac{\omega_1(t)}{2}\sin\frac{\omega_2(t)}{2}\mathbf{e}_1\times\mathbf{e}_2.\end{aligned}$$

Since

$$\dot{\varphi}(t) = -\frac{\frac{1}{2}\dot{\omega}\left[R_1R_2^{-1}\right](t)\cos\frac{\omega\left[R_1R_2^{-1}\right](t)}{2}}{\sin^2\frac{\omega\left[R_1R_2^{-1}\right](t)}{2}},$$

with $\dot{\omega}\left[R_1R_2^{-1}\right](t)$ given by Equation (45),

$$\begin{aligned}\dot{\mathbf{e}}\left[R_1R_2^{-1}\right](t) &= \dot{\varphi}(t)\mathbf{q}(t)+\varphi(t)\dot{\mathbf{q}}(t)\\ &= \frac{1}{\sin^2\frac{\omega\left[R_1R_2^{-1}\right](t)}{2}}\left(\sin\frac{\omega\left[R_1R_2^{-1}\right](t)}{2}\dot{\mathbf{q}}(t)-\frac{1}{2}\dot{\omega}\left[R_1R_2^{-1}\right](t)\cos\frac{\omega\left[R_1R_2^{-1}\right](t)}{2}\mathbf{q}(t)\right),\end{aligned}$$

where

$$\begin{aligned}\dot{\mathbf{q}}(t) &= \frac{d}{dt}\left(\cos\frac{\varpi_2 t}{2}\sin\frac{\varpi_1 t}{2}\mathbf{e}_1-\cos\frac{\varpi_1 t}{2}\sin\frac{\varpi_2 t}{2}\mathbf{e}_2-\sin\frac{\varpi_1 t}{2}\sin\frac{\varpi_2 t}{2}\mathbf{e}_1\times\mathbf{e}_2\right)\\ &= \left(\frac{\varpi_1}{2}\cos\frac{\varpi_1 t}{2}\cos\frac{\varpi_2 t}{2}-\frac{\varpi_2}{2}\sin\frac{\varpi_1 t}{2}\sin\frac{\varpi_2 t}{2}\right)\mathbf{e}_1+\left(\frac{\varpi_1}{2}\sin\frac{\varpi_1 t}{2}\sin\frac{\varpi_2 t}{2}-\frac{\varpi_2}{2}\cos\frac{\varpi_1 t}{2}\cos\frac{\varpi_2 t}{2}\right)\mathbf{e}_2\\ &\quad-\left(\frac{\varpi_1}{2}\cos\frac{\varpi_1 t}{2}\sin\frac{\varpi_2 t}{2}+\frac{\varpi_2}{2}\sin\frac{\varpi_1 t}{2}\cos\frac{\varpi_2 t}{2}\right)\mathbf{e}_1\times\mathbf{e}_2.\end{aligned} \tag{46}$$

The temporal derivatives in the general case would be more involved and cumbersome to present, but not prohibitive of computation.

5.5 | Tectonic plate circuit

Slightly generalizing Equation (20) derived in Section 4.2, the approximation of the transient relative rotation vector $\omega_{1\bar{2}}(t)\mathbf{e}_{1\bar{2}} \approx \omega_1(t)\mathbf{e}_1 - \omega_2(t)\mathbf{e}_2$ implies

$$\dot{\omega}_{1\bar{2}}(t)\mathbf{e}_{1\bar{2}} \approx \dot{\omega}_1(t)\mathbf{e}_1 - \dot{\omega}_2(t)\mathbf{e}_2,$$

that is, the vector of the relative instantaneous angular velocity is approximately equal to the difference of the vectors of absolute instantaneous angular velocity with respect to stationary or instantaneous rotation axes. Then, taking temporal derivatives of the initial plate-circuit expression, Equation (22), yields

$$\boldsymbol{\omega}_{1\bar{2}} + \boldsymbol{\omega}_{2\bar{3}} + \ \dots \ + \boldsymbol{\omega}_{n\bar{1}} \approx \mathbf{0}, \tag{47}$$

stating that the sum of relative instantaneous angular velocity vectors approximately vanishes. Omitting the approximation inherent in Equation (47) and taking it as an equation, it has been referred to as tectonic plate circuit in terms of relative angular velocity vectors ever since [2, 15, 16]. Referring to infinitesimal rotations and an infinitesimal circuit about a triple junction, the equation is presented for $n = 3$ as an easy spherical extension of classical mechanics in the plane in [16, eq. (2), p. 1277], in any case without proof as conceded by the authors in [15, eq. (3), p. 286]. For a unique vector $\mathbf{u}(t) \in \mathbb{S}^3$ subject to all rotations $R_i, i = 1, \dots, n$, the previous Equation (47) implies

$$\boldsymbol{\omega}_{1\bar{2}} \times \mathbf{u}(t) + \boldsymbol{\omega}_{2\bar{3}} \times \mathbf{u}(t) + \ \dots \ + \boldsymbol{\omega}_{n\bar{1}} \times \mathbf{u}(t) \approx \mathbf{0}, \tag{48}$$

that is, the sum of relative instantaneous trajectoral velocities approximately vanishes. Interestingly enough, a term as one of the terms on the left-hand side of Equation (48) defining an instantaneous relative trajectoral velocity was used as the basis of the derivation of Equation (47) in [15, eq. (7), p. 287].

Summing up, transient absolute rotations with respect to a fixed reference frame, for example, a fixed coordinate system for simplicity, determine their corresponding transient relative rotations. A transient absolute and a corresponding transient relative rotation determine the other transient absolute rotation corresponding to the transient relative rotation. Moreover, plate-circuit arguments may apply to determine relative transient rotations from other relative transient rotations.

The general assumption is that the rotating plates do not interact.

5.6 | Inventory of spherical kinematics of plate tectonics

Table 2 compiles the inventory of kinematic modeling of the motion of tectonic plates and aims at clarifying its terms and notation and their relationships.

6 | GEOLOGICAL APPLICATION OF PIECEWISE AND CONTINUOUS KINEMATIC MODELING OF CIRCULAR MOTION ON THE SPHERE

The versatile practicability of the mathematical tools of quantitative spherical kinematics of plate tectonics as provided here is exemplified by two geological applications. The first example features a numerical application of a plate-circuit argument to determine the migrating relative Euler pole of the relative rotation of two plates with respect to each other given their rotations with respect to a third plate about Euler poles referred to as absolute, as they are assumed to be fixed. The second example presents an involved interplay of incremental and accumulating modeling inducing split–join cycles to approximate an observed pattern of sinusoidal geological trajectories as reported by [17], compare Figure 8, and [18] to record the Gondwana breakup.

6.1 | Three-plate problem and its migrating Euler pole by numerical resolution of a plate circuit

Using the spherical deformation pattern of the continents, compare [19], plate tectonic conditions in the early Paleozoic were reconstructed by Kroner et al. [20, 21]. During the formation of the supercontinent Pangea, the continents Gondwana

TABLE 2 Inventory of spherical kinematics of plate tectonics.

Symbol	Meaning
$\mathbf{u}, \mathbf{w}$	Unit vectors in $\mathbb{S}^2 \subset \mathbb{R}^3$, for example, vertices of spherical polygons
R	*Finite* rotation in $\mathbb{R}^3$, for example, $\mathbf{w} = R\mathbf{u}$
$R(\omega, \mathbf{e})$	Rotation parametrized in terms of angle $\omega \in (-\pi, \pi]$ and axis $\mathbf{e} \in \mathbb{S}^2 \subset \mathbb{R}^3$
	Piecewise circular motion *by temporally indexed successive concatenation*
$\tau_0 < \tau_1 < \ldots < \tau_i < \ldots$	Increasing sequence of real discrete temporal marks $\tau_i, i = 1, 2, \ldots$
$R_i = R(\omega(\tau_i), \mathbf{e}(\tau_i))$	Sequence of temporally indexed rotations $R_i, i = 1, 2, \ldots$
$R^{(\ell)} = R_\ell R_{\ell-1} \ldots R_1$	Concatenation of rotations $R_i, i = 1, 2, \ldots, \ell$
$\Delta\tau_i = \tau_i - \tau_{i-1}, i = 1, 2, \ldots$	Finite time lags
$\boldsymbol{\omega}_i = \omega_i \mathbf{e}_i$	Rotation vector associated with $R(\omega_i, \mathbf{e}_i), i = 1, 2, \ldots$
$\boldsymbol{\varpi}_i = (1/\Delta\tau_i)\omega_i \mathbf{e}_i$	Vector of the *mean* angular velocity in $(\tau_{i-1}, \tau_i]$ associated with $R_i = R(\omega_i, \mathbf{e}_i)$ changing the orientation from R_{i-1} to $R_i, i = 1, 2, \ldots$
$\|\boldsymbol{\varpi}_i\| = \omega_i/\Delta\tau_i = \varpi$	*Mean* rotation rate associated with $R_i = R(\omega_i, \mathbf{e}_i)$
$\mathbf{v}_i = \boldsymbol{\varpi}_i \times \mathbf{u}_i$	Vector of the *mean* velocity of $\mathbf{u}_i$ tangential to its small circle of rotation in $(\tau_{i-1}, \tau_i], i = 1, 2, \ldots$
	Continuous rotation *in terms of time-dependent quaternion*
$R(\omega(t), \mathbf{e}(t))$	*Transient* rotation $\mathbf{u}(t) = R(\omega(t), \mathbf{e}(t))\ \mathbf{u}(t_0), t \in [t_0, \infty)$
$\boldsymbol{\omega}(t) = \omega(t)\mathbf{e}(t)$	*Instantaneous* rotation vector associated with $R(\omega(t), \mathbf{e}(t))$
$\dot{\omega}(t)$	*Instantaneous* rotation rate associated with $R(\omega(t), \mathbf{e}(t))$
$\dot{\boldsymbol{\omega}}(t)$	Vector of the *instantaneous* angular velocity $\dot{\boldsymbol{\omega}}(t) = 2\dot{q}(t) \circ q^*(t)$
$\mathbf{v}(t) = \dot{\boldsymbol{\omega}}(t) \times \mathbf{u}(t)$	Vector of the *instantaneous* trajectoral velocity of $\mathbf{u}(t)$ tangential to its small circle of rotation

(GON) and North America (NAC) converged towards Eastern Europe (EEC) for a period of 70 Ma from 500 to 430 Ma. This convergence is coeval with their mutual divergence, which in turn resulted in the formation of the Rheic Ocean, compare Figure 5.

Euler poles $\mathbf{e}_{\mathrm{GON}}$ and $\mathbf{e}_{\mathrm{NAC}}$ of Gondwana's and North America's relative rotational motion with respect to Eastern Europe considered to be immobile were assumed to be stationary and determined by constructive geological reasoning [20, 21]. The corresponding geological reconstruction revealed a complex path of migrating Euler poles describing the divergent motion of Gondwana relative to North America during a time span of 70 Ma. Such a hitherto unexplained migration path of Euler poles is described abstractly here in Section 4.3. Given stationary axes of rotation of Gondwana and North America, respectively, the relative rotation of Gondwana with respect to North America or vice versa requires a transient axis of rotation, that is, a migrating Euler pole $\mathbf{e}_{\mathrm{MEP}}$.

The counterclockwise rotation $R_{\mathrm{EEC}}(\varpi_{\mathrm{GON}}\, t, \mathbf{e}_{\mathrm{GON}})$ of GON with respect to EEC by the constant rotational rate of $\varpi_{\mathrm{GON}} = 1.23\,(°/\mathrm{Ma})$ about the stationary Euler pole $\mathbf{e}_{\mathrm{GON}}$ with geographical coordinates (13.3[°lat], −23.9[°lon]), and the counterclockwise rotation $R_{\mathrm{EEC}}(\varpi_{\mathrm{NAC}}\, t, \mathbf{e}_{\mathrm{NAC}})$ of NAC with respect to EEC by the constant rotational rate of $\varpi_{\mathrm{NAC}} = 0.42$ (°/Ma) about the stationary Euler pole $\mathbf{e}_{\mathrm{NAC}}$ with geographical coordinates (77.6[°lat], 61.9[°lon]) are given. Then, the transient rotation $R_{\mathrm{NAC}}\,(\omega_{\mathrm{MEP}}(t), \mathbf{e}_{\mathrm{MEP}}(t))$ of GON with respect to NAC is determined by the plate-circuit argument, Equation (21), written symbolically as $({}_{\mathrm{GON}}R_{\mathrm{NAC}})\,({}_{\mathrm{NAC}}R_{\mathrm{EEC}})\,({}_{\mathrm{EEC}}R_{\mathrm{GON}}) = I$. In terms of properly parametrized rotations dropping the subscripts, it reads

$$R\,(\omega_{\mathrm{MEP}}(t), \mathbf{e}_{\mathrm{MEP}}(t))\ \ R\,(\varpi_{\mathrm{NAC}}\, t, \mathbf{e}_{\mathrm{NAC}})\ \ (R\,(\varpi_{\mathrm{GON}}\, t, \mathbf{e}_{\mathrm{GON}}))^{-1} = I$$

and leads to

$$R\,(\omega_{\mathrm{MEP}}(t), \mathbf{e}_{\mathrm{MEP}}(t)) = R\,(\varpi_{\mathrm{GON}}\, t, \mathbf{e}_{\mathrm{GON}})\ (R\,(\varpi_{\mathrm{NAC}}\, t, \mathbf{e}_{\mathrm{NAC}}))^{-1},$$

the numerical evaluation of which is summarized in Table 3 and visualized in Figure 5.

The path of migrating Euler poles as depicted in Figure 5 consists of Euler poles of relative rotations with respect to accumulated rotations about fixed Euler poles $\mathbf{e}_{\mathrm{GON}}$ and $\mathbf{e}_{\mathrm{NAC}}$, accumulated in the time spans $(500, T_{\mathrm{Age}}]$, $T_{\mathrm{Age}} = 495{,}490, \ldots, 430$, that is, of Euler poles of the relative rotations $R\left(1.23\,(500 - T_{\mathrm{Age}}), \mathbf{e}_{\mathrm{GON}}\right)$

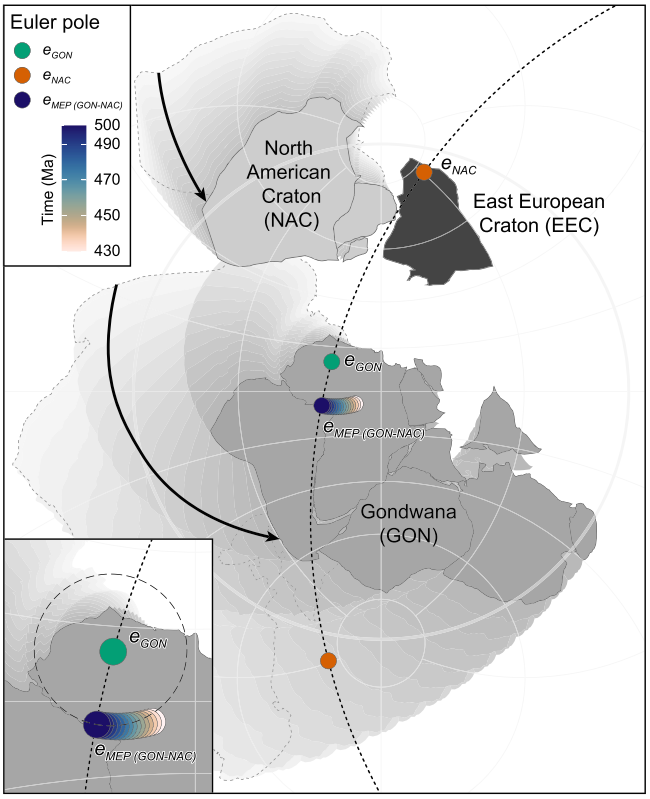

FIGURE 5 Numerical application of a plate-circuit argument to resolve a three-plate problem of early Paleozoic plate tectonics [20, 21]. From 500 to 430 Ma, Gondwana and North America were rotated relative to the East European Craton about stationary Euler poles $\mathbf{e}_{\mathrm{GON}}$ (green bullet) and $\mathbf{e}_{\mathrm{NAC}}$ (red bullet), respectively. At 500 Ma, Gondwana rotated relative to North America about the relative Euler pole $\mathbf{e}_{\mathrm{MEP}}$ located close to the pseudo Euler pole, compare Equation (32), on the great circle spanned by $\mathbf{e}_{\mathrm{GON}}$ and $\mathbf{e}_{\mathrm{NAC}}$. According to proceedingly accumulated total rotations of Gondwana and North America about their stationary Euler poles, the Euler pole of their relative rotation migrates away from the pseudo Euler pole along a path as indicated by a sequence of $\mathbf{e}_{\mathrm{MEP}}$ (colored bullets). It is emphasized that the relative Euler pole does not migrate along any small circle centered at $\mathbf{e}_{\mathrm{GON}}$ (inset at lower left). [Colour figure can be viewed at wileyonlinelibrary.com]

$\left(R\left(0.42(500-T_{\mathrm{Age}}),\mathbf{e}_{\mathrm{NAC}}\right)\right)^{-1}$, $T_{\mathrm{Age}} = 495{,}490, \ldots, 430$. The first Euler pole assigned to $T_{\mathrm{Age}} = 500$ along the path of migration is the stationary Euler pole of the relative rotation $R(1.23,\mathbf{e}_{\mathrm{GON}})\,(R(0.42,\mathbf{e}_{\mathrm{NAC}}))^{-1}$ of the incremental rotations $R(1.23,\mathbf{e}_{\mathrm{GON}})$ and $R(0.42,\mathbf{e}_{\mathrm{NAC}})$ corresponding to a time lag of 1 Ma. Since the rates ϖ_{GON} and ϖ_{NAC} are small, the incremental relative Euler pole is close to the pseudo Euler pole, Equation (19), on the great circle spanned by $\mathbf{e}_{\mathrm{GON}}$ and $\mathbf{e}_{\mathrm{NAC}}$.

Since the plate-circuit argument has been derived from properties of rotations featuring sufficiently small angles of rotation, this example suggests that the motion of the migrating relative Euler pole is not driven by geodynamics but merely depends on the chosen reference frame, that is, on the point of view.

6.2 | Modeling of sinusoidal trajectories

Two spherical polygons assumed to model the geometry of two divergent tectonic plates with a common segment of boundary are subject to incremental rotational motions R_1 and R_2 (cf. Section 5.2.1 and Figure 2) about two different fixed absolute Euler poles $\mathbf{e}_1$ and $\mathbf{e}_2$ with different rotational rates resulting in relative orientations $R_1R_2^{-1}$ and $R_2R_1^{-1}$ unique up to the sign of their rotation vectors. Interleaving the successive incremental rotations and the relative rotation gives rise to split–join cycles. If the trajectories of the progressing relative rotations of the successively incrementally rotated common boundary segment are traced on the plates while being rotated, these traces are of sinusoidal shape, where sinusoidal is meant as a rough qualitative description rather than a properly parametrized expression.

6.2.1 | Piecewise modeling of sinusoidal trajectories

The plates' absolute motion is to be modeled in terms of two sequences of successive incremental finite rotations $R_1 = R(\omega_1,\mathbf{e}_1)$ and $R_2 = R(\omega_2,\mathbf{e}_2)$, respectively, corresponding to temporal lags of 1 Ma such that $\omega_1 = |\varpi_1|(^\circ)$, $\omega_2 = |\varpi_2|(^\circ)$.

TABLE 3 Summary of numerical application of plate circuit.

Age (Ma)	ω_{GON} (°)	ω_{NAC} (°)	ω_{MEP} (°)	$\Delta\omega_{MEP}$ (°)	$\dot{\omega}_{MEP}$ (°)	lat MEP (°)	lon MEP (°)	θ (rad)	$\|\dot{\mathbf{e}}_{MEP}\|$ (l)
500	1.230	0.420	1.201	1.201	1.201	−6.128	−28.016	NA	0.004
495	6.150	2.100	6.002	1.200	1.200	−6.292	−27.191	0.004	0.004
490	12.300	4.200	12.003	1.200	1.200	−6.465	−26.154	0.004	0.004
485	18.450	6.300	17.999	1.199	1.199	−6.602	−25.108	0.004	0.004
480	24.600	8.400	23.990	1.198	1.197	−6.705	−24.053	0.004	0.004
475	30.750	10.500	29.972	1.196	1.196	−6.771	−22.990	0.004	0.004
470	36.900	12.600	35.945	1.194	1.193	−6.801	−21.919	0.004	0.004
465	43.050	14.700	41.905	1.192	1.191	−6.794	−20.840	0.004	0.004
460	49.200	16.800	47.850	1.189	1.188	−6.749	−19.751	0.004	0.004
455	55.350	18.900	53.779	1.186	1.184	−6.667	−18.655	0.004	0.004
450	61.500	21.000	59.690	1.182	1.180	−6.545	−17.550	0.004	0.004
445	67.650	23.100	65.579	1.178	1.176	−6.384	−16.436	0.004	0.004
440	73.800	25.200	71.444	1.173	1.171	−6.182	−15.314	0.004	0.004
435	79.950	27.300	77.284	1.168	1.165	−5.938	−14.183	0.004	0.004
430	86.100	29.400	83.094	1.162	1.159	−5.651	−13.044	0.004	0.004

Note: col 1: geological age T_{Age}; col 2: cumulative angle ω_{GON} of rotating GON with respect to EEC; col 3: cumulative angle ω_{NAC} of rotating NAC with respect to EEC; col 4: accumulated total angle ω_{MEP} of rotating GON with respect to NAC about migrating Euler pole $\mathbf{e}_{MEP}$; col 5: difference $\Delta\omega_{MEP} = (\omega_{MEP}(T_{Age}) - \omega_{MEP}(T_{Age} + \Delta t))/\Delta t$ of cumulative angles of rotation per time step $\Delta t = 5$; col 6: instantaneous angular velocity $\dot{\omega}_{MEP}$ of rotation about migrating Euler pole $\mathbf{e}_{MEP}$; col 7: latitude of migrating Euler pole $\mathbf{e}_{MEP}$; col 8: longitude of migrating Euler pole $\mathbf{e}_{MEP}$; col 9: angle $\theta = \angle(\mathbf{e}_{MEP}(T_{Age}), \mathbf{e}_{MEP}(T_{Age} + \Delta t))/\Delta t$ of successive locations of migrating Euler pole per time step; col 10: scalar instantaneous trajectoral velocity $\|\dot{\mathbf{e}}_{MEP}\|$ of Euler pole $\mathbf{e}_{MEP}$ migrating along its path.

For each temporal lag, the relative motion of the two plates with respect to each other is modeled by $R_1R_2^{-1}$ or $\left(R_1R_2^{-1}\right)^{-1} = R_2R_1^{-1}$, compare Section 5.2.1, which differ by the sign of their rotation vector, that is, either by the sign of their Euler pole or by the sign of their angle of rotation.

The two spherical plates are assumed to initially have a common segment of boundary B_0 given by an arc of a great circle because edges of spherical polygons are arcs of great circles by definition. It is depicted in black in all of Figure 6. The shape of the common boundary segment is actually not critical here. Eight points have been placed equidistantly along the boundary segment to visualize individual trajectories.

The rotations $R_1 = R(\omega_1, \mathbf{e}_1)$ and $R_2 = R(\omega_2, \mathbf{e}_2)$ are defined by angles $\omega_1 = 30(°), \omega_2 = 15(°)$ and Euler poles $\mathbf{e}_1$ and $\mathbf{e}_2$ as shown in Figure 6 as green and red bullets, respectively. The angles and accordingly the rates have been exaggeratedly enlarged for the purpose of proper visualization only.

In the first step these rotations are applied to the two plates with special attention paid to their effect on the initial common boundary segment B_0 depicted in black. The common boundary segment B_0 is split into two diverging margins $M_{11} = R_1B_0$ and $M_{12} = R_2B_0$ depicted in green and red, respectively, in Figure 6A,B. For the eight points along the initial boundary segment B_0, the rotational trajectories with respect to R_1 and R_2, respectively, are correspondingly visualized as green or red small circle arcs, compare in Figure 6A,B.

The Euler pole $\mathbf{e}_r$ of the relative rotations

$$R_1R_2^{-1} = R_{1\bar{2}} = R(\omega_r, \mathbf{e}_r) \quad \text{and} \quad \left(R_1R_2^{-1}\right)^{-1} = R_2R_1^{-1} = R_{2\bar{1}} = R(-\omega_r, \mathbf{e}_r),$$

respectively, is shown as blue bullet. The trajectories of the corresponding relative rotation with angle ω_r are shown as blue small circle arcs linking the margins M_{11} and M_{12} by virtue of $R_1R_2^{-1}M_{12} = R_{1\bar{2}}M_{12} = M_{11}$ or $R_2R_1^{-1}M_{11} = R_{2\bar{1}}M_{11} = M_{12}$, respectively, compare Figure 6B. The union of these trajectories constitutes the pattern $\mathcal{P}_1$.

To keep the notation tidy, the rotations

$$Q_p = R\left(p\omega_r, \mathbf{e}_r\right) \quad \text{and} \quad \overline{Q}_p = R\left((p-1)\omega_r, \mathbf{e}_r\right), 0 < p < 1, \tag{49}$$

are defined. They decompose $R_{1\bar{2}}$ and $R_{2\bar{1}}$, respectively, such that

$$R_{1\bar{2}} = Q_p\overline{Q}_p^{-1} = \overline{Q}_p^{-1}Q_p, R_{2\bar{1}} = \overline{Q}_pQ_p^{-1} = Q_p^{-1}\overline{Q}_p,$$

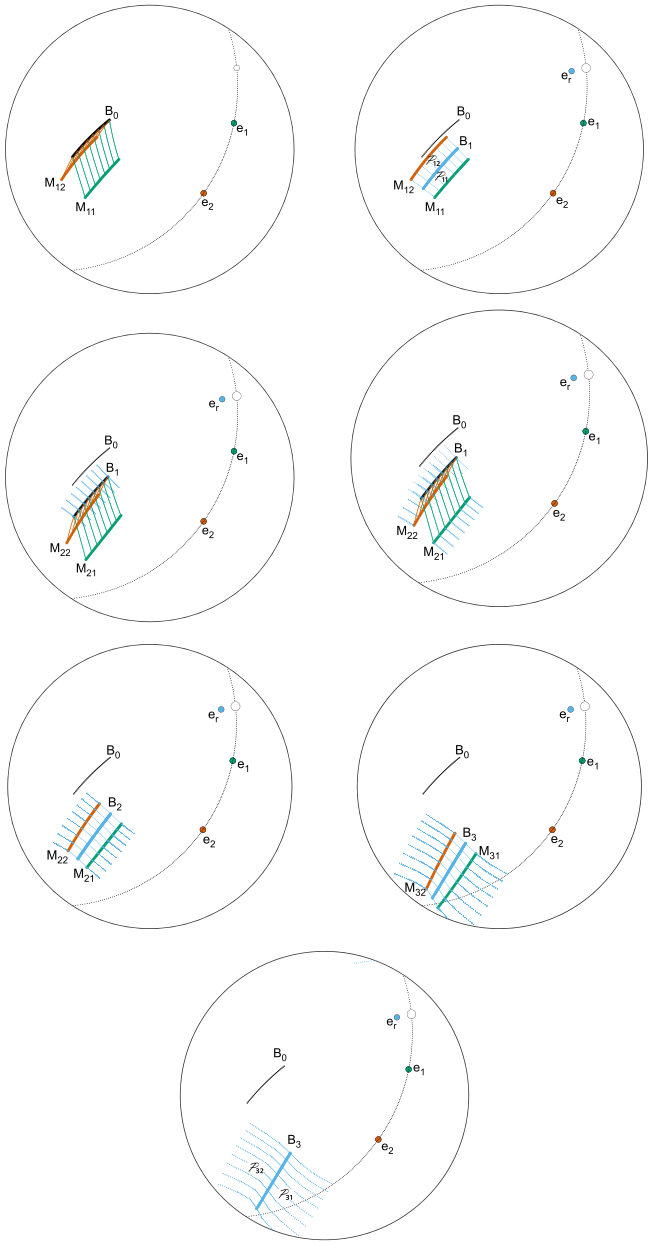

FIGURE 6 Three successive temporal steps of 1 Ma each of piecewise motion in terms of incremental rotations with rates $\varpi_1 = 30(°/\text{Ma})$, $\varpi_2 = 15(°/\text{Ma})$ about fixed absolute Euler poles $\mathbf{e}_1$ (green bullet) and $\mathbf{e}_2$ (red bullet). The location of the corresponding relative Euler pole $\mathbf{e}_r$ is indicated by a blue bullet, the location of the pseudo Euler pole of Equation (8) is indicated by an open circle. Initial setting (top left (A)), details of first step (top right (B), second row (C,D)), second step (third row left (E)), third step (third row right (F)), and final pattern after three steps (bottom center (G)).. [Colour figure can be viewed at wileyonlinelibrary.com]

implying for instance $Q_p R_{2\overline{1}} \overline{Q}_p^{-1} = I$. It should be noted that Q_p and $\overline{Q}_p$ commute and that the angle of rotation $\overline{Q}_p$ is negative, $(p-1)\omega_r < 0$, if $\omega_r > 0$.

Then, a new joint boundary segment B_1 of the two plates intermediate between the margins M_{11} and M_{12} is generated by

$$\begin{aligned} B_1 &= Q_p M_{12} = Q_p R_2 B_0 \\ &= \overline{Q}_p M_{11} = \overline{Q}_p R_1 B_0. \end{aligned}$$

Generating an actual joint boundary in this way roughly simulates growth of both plates by rates of p and $1-p$, respectively, such that their relative location, that is, their relative orientation, is preserved even though the initial plates are torn apart

from each other by rotations R_1 and R_2, respectively. For reasons of simplicity and ease of visualization p was set to $p = \frac{1}{2}$ in this example, and the corresponding new joint boundary segment is depicted in blue in Figure 6B. Each small circle arc linking the margins M_{11} and M_{12} may be split into two partial arcs linking M_{11} and B_1 and M_{12} and B_1. The pattern comprising all partial arcs linking M_{11} and B_1 is referred to as $\mathcal{P}_{11}$, the pattern comprising all partial arcs linking M_{12} and B_1 is referred to as $\mathcal{P}_{12}$, and $\mathcal{P}_{11} \cup \mathcal{P}_{12} = \mathcal{P}_1$.

In the second step, the current boundary segment B_1 and the pattern $\mathcal{P}_{11}$ are rotated by R_1 resulting a new margin $M_{21} = R_1 B_1 = R_1 \overline{Q}_p R_1 B_0$ (green line of Figure 6C) and $R_1 \mathcal{P}_{11}$ (blue lines of Figure 6D) and analogously in another new margin $M_{22} = R_2 B_1 = R_2 Q_p R_2 B_0$ and $R_2 \mathcal{P}_{12}$ (Figure 6C,D). Thus, the current boundary segment B_1 is split into two diverging margins M_{21} and M_{22}. The trajectories of the rotation R_1 about $\mathbf{e}_1$ and of the rotation R_2 about $\mathbf{e}_2$ are plotted as green and red small circle arcs in Figures 6C,D. The current margins M_{21} and M_{22} spawn a new incremental pattern $\mathcal{P}_2$ consisting of trajectories of the relative rotations $R_{2\bar{1}}$ and $R_{1\bar{2}}$, respectively, mapping M_{21} to M_{22} and vice versa. The pattern $\mathcal{P}_2$ may be thought of as divided into two partial patterns $\mathcal{P}_{21}$ and $\mathcal{P}_{22}$ with respect to the next new joint boundary segment

$$\begin{aligned} B_2 &= Q_p M_{22} = Q_p R_2 B_1 = Q_p R_2 Q_p R_2 B_0 = \left(Q_p R_2\right)^{(2)} B_0 \\ &= \overline{Q}_p M_{21} = \overline{Q}_p R_1 B_1 = \overline{Q}_p R_1 \overline{Q}_p R_1 B_0 = \left(\overline{Q}_p R_1\right)^{(2)} B_0, \end{aligned}$$

intermediate between M_{21} and M_{22} as shown in Figure 6E. A parenthesized superscript of a rotation indicates manifold concatenation of the rotation with itself. At this stage, the entire pattern of trajectories initially originating from relative rotations about $\mathbf{e}_r$ comprises the two partial patterns $R_1 \mathcal{P}_{11} \cup \mathcal{P}_{21}$ and $R_2 \mathcal{P}_{12} \cup \mathcal{P}_{22}$.

In each consecutive step, the previous partial patterns to be rotated by R_1 or R_2, respectively, are extended by the union of new partial incremental patterns $\mathcal{P}_{\ell 1}$ and $\mathcal{P}_{\ell 2}$, respectively, resulting from dividing $\mathcal{P}_\ell$ with respect to the actual joint boundary segment B_ℓ.

Thus, in the nth step, the actual diverging margins

$$M_{n1} = R_1 B_{n-1} = R_1 \left(\overline{Q}_p R_1\right)^{(n-1)} B_0, \tag{50}$$

$$M_{n2} = R_2 B_{n-1} = R_2 \left(Q_p R_2\right)^{(n-1)} B_0, n \in \mathbb{N}, \tag{51}$$

imply the new incremental pattern $\mathcal{P}_n$ consisting of trajectories of the relative rotations $R_{2\bar{1}}$ and $R_{1\bar{2}}$ mapping M_{n1} to M_{n2}, $\left(R_2 R_1^{-1}\right) M_{n1} = \left(R_2 R_1^{-1}\right) R_1 B_{n-1} = R_2 B_{n-1} = M_{n2}$, and vice versa. It should be noted that M_{ni} is not the result of an $(n-1)$-fold rotation of B_0 by $R_i, i = 1, 2$. Nevertheless, Equations (50) and (51) may be read as accumulating successive concatenation of finite rotations, such that the actual margins M_{n1} and M_{n2} are related by

$$\begin{aligned} M_{n2} &= \left(R_2 \left(Q_p R_2\right)^{(n-1)}\right) \left(R_1 \left(\overline{Q}_p R_1\right)^{(n-1)}\right)^{-1} M_{n1} \\ &= R_2 \underbrace{Q_p R_2 \ \ldots \ Q_p R_2}_{n-1} R_1^{-1} \overline{Q}_p^{-1} \ \ldots \ R_1^{-1} \overline{Q}_p^{-1} R_1^{-1} M_{n1} \\ &= R_2 R_1^{-1} M_{n1}, n \in \mathbb{N}, \end{aligned}$$

that is, their relative location is the same for all $n \in \mathbb{N}$.

The actual joint boundary segment

$$B_n = \overline{Q}_p M_{n1} = \left(\overline{Q}_p R_1\right) B_{n-1} = \left(\overline{Q}_p R_1\right)^{(n)} B_0 \tag{52}$$

$$= Q_p M_{n2} = \left(Q_p R_2\right) B_{n-1} = \left(Q_p R_2\right)^{(n)} B_0, n \in \mathbb{N}, \tag{53}$$

in between the margins M_{n1} and M_{n2} can be seen as the result of the rotation of B_0 by the n-fold concatenation of $\overline{Q}_p R_1$ or $Q_p R_2$, respectively. It divides the pattern $\mathcal{P}_n$ into two partial patterns $\mathcal{P}_{n1}$ and $\mathcal{P}_{n2}$ associated with M_{n1} and M_{n2}, compare Figure 6F. Equations (52) and (53) imply the relationships

$$M_{n1} = \overline{Q}_p^{-1} B_n \quad \text{and} \quad M_{n2} = Q_p^{-1} B_n, \tag{54}$$

expressing the diverging margins M_{n1} and M_{n2} in terms of the current joint boundary segment B_n and the n-fold rotations $(\overline{Q}_p R_1)^{(n)}$ and $(Q_p R_2)^{(n)}$.

Eventually, at the nth stage, the two partial patterns are

$$\begin{aligned} &\mathcal{P}_{n1} \cup R_1 \mathcal{P}_{(n-1)1} \cup R_1^{(2)} \mathcal{P}_{(n-2)1} \cup \ \dots \ \cup R_1^{(n-2)} \mathcal{P}_{21} \cup R_1^{(n-1)} \mathcal{P}_{11} \\ &= \mathcal{P}_{n1} \cup \bigcup_{\ell=1}^{n-1} R_1^{(\ell)} \mathcal{P}_{(n-\ell)1} = \mathcal{P}_{n1} \cup \bigcup_{\ell=1}^{n-1} R(\ell\omega_1, \mathbf{e}_1) \mathcal{P}_{(n-\ell)1}, \end{aligned} \tag{55}$$

and analogously

$$\begin{aligned} &\mathcal{P}_{n2} \cup R_2 \mathcal{P}_{(n-1)2} \cup R_2^{(2)} \mathcal{P}_{(n-2)2} \cup \ \dots \ \cup R_2^{(n-2)} \mathcal{P}_{22} \cup R_2^{(n-1)} \mathcal{P}_{12} \\ &= \mathcal{P}_{n2} \cup \bigcup_{\ell=1}^{n-1} R_2^{(\ell)} \mathcal{P}_{(n-\ell)2} = \mathcal{P}_{n2} \cup \bigcup_{\ell=1}^{n-1} R(\ell\omega_2, \mathbf{e}_2) \mathcal{P}_{(n-\ell)2}, \end{aligned} \tag{56}$$

where the respective last equalities hold if the Euler poles $\mathbf{e}_1$ and $\mathbf{e}_2$ are stationary as assumed in this example.

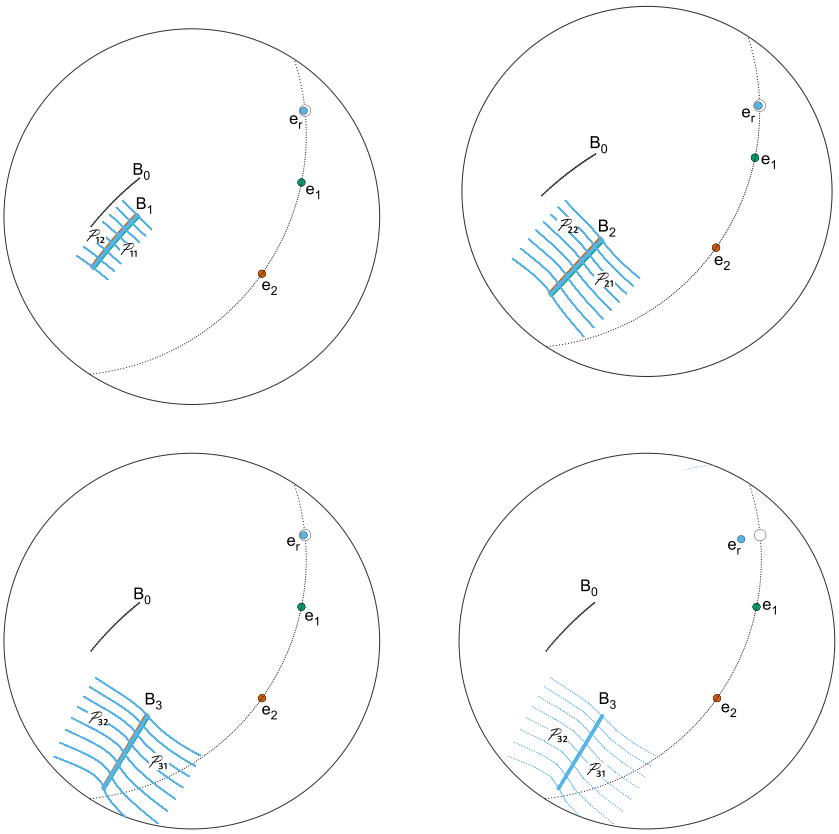

FIGURE 7 Three temporal states of pattern of sinusoidal trajectories after 15 (top left (A)), 30 (top right (B)), and 45 Ma (bottom left (C)) of piecewise motion in terms of incremental rotations with rates $\varpi_1 = 2.0(°/\text{Ma})$, $\varpi_2 = 1.0(°/\text{Ma})$ about fixed absolute Euler poles $\mathbf{e}_1$ (green bullet) and $\mathbf{e}_2$ (red bullet). The location of the corresponding relative Euler pole $\mathbf{e}_r$ is indicated by a blue bullet very close to the pseudo Euler pole of Equation (8) (open circle ∘). Pattern (bottom right (D)) as displayed in Figure 6G for quick comparison. [Colour figure can be viewed at wileyonlinelibrary.com]

The union of all patterns of Equations (55) and (56) displayed in Figure 6G resembles the sinusoidal shape of flow lines as observed by [17], compare Figure 8, and [18] to record the relative Jurassic motion of the plates of Africa and Madagascar–Antarctica.

Figure 7 illustrates the same model for smaller rotation rates $\varpi_1 = 2.0(°/\text{Ma})$ and $\varpi_2 = 1.0(°/\text{Ma})$. Modeling as before for temporal lags of 1 Ma such that the angles of rotation are $\omega_1 = 2.0(°)$ and $\omega_2 = 1.0(°)$, the corresponding relative Euler pole (blue bullet) is much closer to the pseudo Euler pole of Equation (8) (open circle) located on the great circle spanned by the two absolute Euler poles (green and red bullets). To evolve the patterns of sinusoidal trajectories as before, the model requires more incremental steps to cover the same total period of time. Actually, the states after 15, 30, and 45 Ma are displayed in Figure 7A–C, Figure 7D repeats Figure 6G for immediate comparison.

6.2.2 | Continuous modeling of sinusoidal trajectories

The cumulative notation of Equations (50), (51), and (54) suggests a rephrasing of the model in terms of continuous rotations assuming as before fixed Euler poles $\mathbf{e}_i$, $i = 1, 2$, and constant rotation rates ϖ_i such that $\omega_i(t) = t\varpi_i$, $i = 1, 2$. Replacing the counter n of proceeding steps by a continuous variable $t \in [0, \infty)$ representing time leads to $R_i(t) = R_i(t\varpi_i, \mathbf{e}_i)$, $i = 1, 2$, and $Q_p(t) = R(p\omega_r(t), \mathbf{e}_r)$ and $\overline{Q}_p(t) = R((p-1)\omega_r(t), \mathbf{e}_r)$ corresponding to Equation (49). Then, the continuous model reads

$$B(t) = \overline{Q}_p(t)R_1(t)B_0 = Q_p(t)R_2(t)B_0, \tag{57}$$

$$M_1(t) = \overline{Q}_p^{-1}(\Delta t)B(t), \tag{58}$$

$$M_2(t) = Q_p^{-1}(\Delta t)B(t), t \in [0, \infty), \tag{59}$$

where Equation (57) represents the instantaneous joint boundary segment $B(t)$ split into the instantaneous divergent margins $M_1(t)$ and $M_2(t)$ represented by Equations (58) and (59) implying as before $M_2(t) = R_2(\Delta t)R_1^{-1}(\Delta t)M_1(t)$. The complete pattern $\mathcal{P}(t)$ of trajectories at time $t > 0$ depends on the lengths of split–join cycles and their total number during

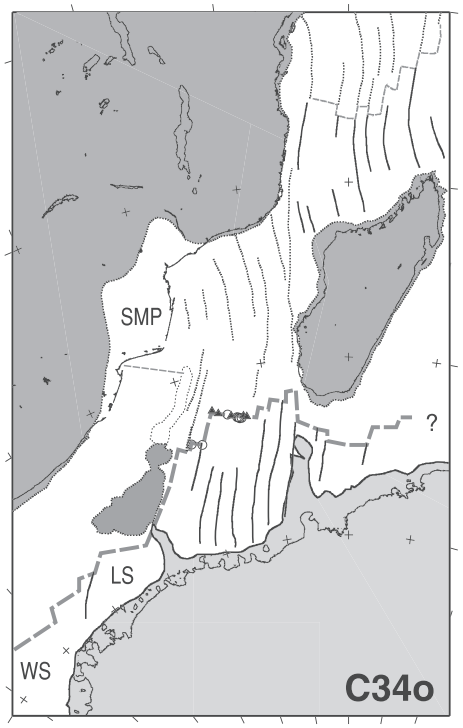

FIGURE 8 Plate tectonic constellation 125 Ma ago. Africa (upper left) and Madagascar–Antarctica (lower right) represent the plates of West and East Gondwana, respectively. The Mesozoic breakup of Gondwana resulted in the opening of oceanic basins due to sea floor spreading at the divergent plate boundaries and left the pattern of sinusoidal flow lines of the ocean floor as depicted. Figure courtesy of Oxford Journal and the Royal Astronomical Society, fig. 13, C34o, p. 714, from [17], A model of plate kinematics in Gondwana breakup, Geophysical Journal International 173, 703–717. [Colour figure can be viewed at wileyonlinelibrary.com]

the time span $[0, t]$ controlled by the parameter Δt. It comprises the most recent incremental partial patterns and multiple rotated previous partial patterns analogously to the piecewise model.

6.2.3 | Geological perspectives

The continuous model has to be sampled at discrete times to evaluate it numerically. When sampling the continuous model at times corresponding to the time lag of the discrete model, the numerical realizations of the models cannot be distinguished.

Of course, there are more models to approximate and eventually simulate patterns of sinusoidal trajectories. For instance, if the rotational rate ϖ_1 is not constant but increasing, then the relative location of $M_1(t)$ and $M_2(t)$ is no longer stationary but varies with t, and the relative Euler poles migrate along a path close to the great circle spanned by the two absolute Euler poles $\mathbf{e}_1$ and $\mathbf{e}_2$. Considering transient rates $\varpi_1(t) > \varpi_2(t)$ and transient Euler poles $\mathbf{e}_1(t), \mathbf{e}_2(t)$ turns the model only slightly more intricate in terms of its parameters but much more flexible, eventually allowing for the simulation of geologically given patterns of sinusoidal trajectories.

It may be inferred here that extraordinary geological events changing the tectonic regime or sets of jumping Euler poles are not necessarily required to explain and model sinusoidal flow lines as illustrated in Figure 8. More geoscience implications will be elaborated on in a companion paper to be published elsewhere.

7 | CONCLUSIONS

Our communication aims for an overdue update and revision of textbook knowledge as Cox and Hart [13] for instance and completion of the Appendix (277–278) of Le Pichon et al. [2]. Turned constructive, it instructively resolves the three-plate problem in general, and provides a first rough approximation of sinusoidal trajectories of observed motion of tectonic plates for example.

In greater detail

- The terms infinitesimal, instantaneous, and finite rotation are discussed and clarified and an extension to continuous rotations in terms of transient unit quaternions is presented.

  Historically, the mathematical construct of infinitesimal rotations may have been instrumental to develop the notion of instantaneous entities with respect to circular motion on spheres. However, they do not prove suitable to properly model finite rotations or finite rotational motion of tectonic plates numerically. In fact, their application was often flawed by confusing an infinitesimal angle of rotation with a small yet finite angle of rotation. Since small angle approximations provide all it takes, infinitesimal rotations are rendered obsolete for applications to modeling the kinematics of plate tectonics. Mastering fully transient quaternions should finally substantiate to abandon infinitesimal rotations in quantitative plate tectonics.
- The notion of plate circuit is put on sound mathematical grounds and characterized as property of finite rotations. Thus, it is exempted from references to infinitesimal rotations and triple junctions. The required assumptions and corresponding validity of its various forms are clarified and contrasted to textbook representations which must not be read in a strict sense but as implicit approximations. Eventually, it is generalized for transient rotations.
- Two discrete models of circular motion of tectonic plates on the sphere by sequences of (i) incremental finite rotations or (ii) accumulating successive concatenations of finite rotations are presented which are consistent and compatible. They provide different stepwise approximating views of the same motion. In particular, given two plates and their absolute rotations, the models differ in their corresponding relative rotation referring to different spatial references.

  From the point of view of successively accumulating concatenations of finite rotations, the Euler pole of the relative rotation migrates, its motion is not generally along any circle and not uniform. Moreover, the relative rotation about the migrating Euler pole is not uniform, that is, the rotation rate of the relative rotation is not constant albeit constant individual rates of the involved absolute rotations.
- Continuous rotation in terms of time-dependent quaternion and its temporal derivative provide the methodology of a continuous representation of plates' motion and turn its stepwise approximation into a proper yet incomplete view, for example, in terms of mean versus instantaneous angular velocities.
- To explain traces of long-term motions of tectonic plates of more complex shape than, for instance, transform faults aligned with small circle arcs centered at some Euler pole, does not require extraordinary geological events, that is, changes of the tectonic regime. It has been demonstrated here for the first time that the formation of sinusoidal flow

lines and the cause of the migration of Euler poles and its features can be explained and modeled within a unique steady setting. Thus, the paradigm of plate tectonics that traces of long-term motions of plates devise simple geometric patterns as long as the tectonic regime does not change has been questioned in a constructive way.

ACKNOWLEDGEMENTS

The authors gratefully acknowledge approval by Oxford Journal and the Royal Astronomical Society to reuse fig. 13, C34o, p. 714, from [17], A model of plate kinematics in Gondwana breakup, Geophysical Journal International 173, 703–717, as Figure 8. The presentation of Section 5.3 largely follows the undated draft "Sphärische und Räumliche Kinematik" by Wolfgang Ströher accessible in the internet https://www.geometrie.tuwien.ac.at/former/pdf/stroeher_sphaerische_und_raeumliche_kinematik.pdf (visited 230815) only. The authors would like to thank an anonymous reviewer who provided helpful and empathic advice to improve this communication and Bram Vaes for his gentle reminder to pay due attention to the demands of the geoscience community. Open Access funding enabled and organized by Projekt DEAL.

CONFLICT OF INTEREST STATEMENT

The authors declare no potential conflict of interests.

DEDICATION

The authors would like to dedicate their communication to Xavier Le Pichon on the occasion of the 50th anniversary of publication of "Plate Tectonics" (1973) with Jean Francheteau and Jean Bonnin.

ORCID

Helmut Schaeben https://orcid.org/0000-0002-0237-9857

REFERENCES

1. X. Le Pichon, *Fifty years of plate tectonics: afterthoughts of a witness*, Tectonics **38** (2019), 2919–2933, DOI 10.1029/2018TC005350.
2. X. Le Pichon, J. Francheteau, and J. Bonnin, *Plate tectonics: developments in geotectonics*, Elsevier, Amsterdam–London–New York, 1973.
3. O. Rodrigues, *Des lois géométriques qui régissent les déplacements d'un système solide dans l'espace, et de la variation des coordonnées provenant de ses déplacements considérés indépendamment des causes qui peuvent les produire*, J. Math. Pures Appl. Liouville **5** (1840), 380–440.
4. S. L. Altmann, *Rotations, quaternions and double groups*, Clarendon Press, Oxford, 1986.
5. W. R. Hamilton, *On quaternions; or a new system of imaginaries in algebra*, Phil. Mag., 3rd ser. **25** (1844), 489–495.
6. B. K. P. Horn, *Quaternions: what are they, and why do we need to know?* Acta Cryst. **A76** (2020), 556–558.
7. J. Bair, P. Blaszczyk, R. Ely, V. Henry, V. Kanovei, K. U. Katz, M. G. Katz, T. Kudryk, S. S. Kutateladze, T. McGaffey, T. Mormann, D. M. Schaps, and D. Sherry, *Cauchy, infinitesimals and ghosts of departed quantifiers*, Mat. Stud. **47** (2017), 115–144.
8. C. B. Boyer, *The history of the calculus and its conceptual development*, Dover, New York, 1949.
9. H. Schaeben, Quaternions and rotations, *Encyclopedia of mathematical geosciences*, B. S. Daya Sagar, Q. Cheng, J. McKinley, and F. Agterberg, (eds.), Encyclopedia of Earth Sciences Series, Springer, Cham, 2021, DOI 10.1007/978-3-030-26050-7_436-1; visited 230209.
10. J. M. McCarthy and G. S. Soh, Spherical kinematics, *Geometric design of linkages*, 2nd ed., J. M. McCarthy and G. S. Soh, (eds.), Springer, New York, NY, pp. 179–202, 2011, DOI 10.1007/978-1-4419-7892-9_8.
11. J. B. Kuipers, *Quaternions and rotation sequences*, Princeton University Press, Princeton, New Jersey, USA, 1999.
12. P. Wessel and R. D. Müller, Plate tectonics, *Treatise on geophysics*, 2nd ed., G. Schubert, (ed.), Vol. **6**, 2015, pp. 45–93.
13. A. Cox and R. B. Hart, *Plate tectonics: how it works*, Blackwell Scientific Publication, Palo Alto, California, USA, 1986.
14. J. C. K. Chou, *Quaternion kinematic and dynamic differential equations*, IEEE Trans. Robot. Autom. **8** (1992), 53–64.
15. D. P. McKenzie and R. L. Parker, *Plate tectonics in ω-space*, Earth Planet. Sci. Lett. **22** (1974), 285–293.
16. D. P. McKenzie and R. L. Parker, *The North Pacific: an example of tectonics on a sphere*, Nature **216** (1967), 1276–1280, DOI 10.1038/2161276a0.
17. G. Eagles and M. König, *A model of plate kinematics in Gondwana breakup*, Geophys. J. Int. **173** (2008), 703–717, DOI 10.1111/j.1365-246X.2008.03753.x.
18. C. O. Mueller and W. Jokat, *The initial Gondwana break-up: a synthesis based on new potential field data of the Africa-Antarctica Corridor*, Tectonophysics **750** (2018), 301–328, DOI 10.1016/j. tecto.2018.11.008.
19. U. Kroner, M. Roscher, and R. L. Romer, *Ancient plate kinematics derived from the deformation pattern of continental crust: Paleo- and Neo-Tethys opening coeval with prolonged Gondwana-LauRussia convergence*, Tectonophysics **681** (2016), 220–233.

20. U. Kroner, T. Stephan, R. L. Romer, and M. Roscher, Paleozoic plate kinematics during the Pannotia-Pangaea supercontinent cycle, *Pannotia to Pangaea: Neoproterozoic and Paleozoic orogenic cycles in the circum-Atlantic region*, J. B. Murphy, R. A. Strachan, and C. Quesada, (eds.), Geological Society, Special Publications, London, Boulder, Colorado, USA, 2020, pp. 83–104, DOI 10.1144/SP503-2020-15.
21. U. Kroner, T. Stephan, and R. L. Romer, Paleozoic orogenies and relative plate motions at the sutures of the Iapetus-Rheic Ocean, *New developments in the Appalachian-Caledonian-Variscan orogen*, Y. D. Kuiper, J. B. Murphy, R. D. Nance, R. A. Strachan, and M. D. Thompson, (eds.), Vol. **554**, Geological Society of America, 2022, pp. 1–23, DOI 10.1130/2021.2554(01).

How to cite this article: H. Schaeben, U. Kroner, and T. Stephan, *Mathematical fundamentals of spherical kinematics of plate tectonics in terms of quaternions*, Math. Meth. Appl. Sci. (2023), 1–28, DOI 10.1002/mma.9823.